New Jersey Institute of Technology
Digital Commons @ NJIT

Theses | Theses and Dissertations

Spring 2013

Finite element modeling of temperature elevation due to NIR exposure in neural tissue

Atabek Can Yucel
New Jersey Institute of Technology

Follow this and additional works at: https://digitalcommons.njit.edu/theses

Part of the Biomedical Engineering and Bioengineering Commons

Recommended Citation
Yucel, Atabek Can, "Finite element modeling of temperature elevation due to NIR exposure in neural tissue" (2013). *Theses*. 155.
https://digitalcommons.njit.edu/theses/155

This Thesis is brought to you for free and open access by the Theses and Dissertations at Digital Commons @ NJIT. It has been accepted for inclusion in Theses by an authorized administrator of Digital Commons @ NJIT. For more information, please contact digitalcommons@njit.edu.

Copyright Warning & Restrictions

The copyright law of the United States (Title 17, United States Code) governs the making of photocopies or other reproductions of copyrighted material.

Under certain conditions specified in the law, libraries and archives are authorized to furnish a photocopy or other reproduction. One of these specified conditions is that the photocopy or reproduction is not to be "used for any purpose other than private study, scholarship, or research." If a, user makes a request for, or later uses, a photocopy or reproduction for purposes in excess of "fair use" that user may be liable for copyright infringement,

This institution reserves the right to refuse to accept a copying order if, in its judgment, fulfillment of the order would involve violation of copyright law.

Please Note: The author retains the copyright while the New Jersey Institute of Technology reserves the right to distribute this thesis or dissertation

Printing note: If you do not wish to print this page, then select "Pages from: first page # to: last page #" on the print dialog screen

NJIT New Jersey's Science & Technology University

The Van Houten library has removed some of the personal information and all signatures from the approval page and biographical sketches of theses and dissertations in order to protect the identity of NJIT graduates and faculty.

ABSTRACT

FINITE ELEMENT MODELING OF TEMPERATURE ELEVATION DUE TO NIR EXPOSURE IN NEURAL TISSUE

by
Atabek Can Yucel

Near infrared (NIR) lasers have been used in various types of medical applications. Heating is one of the most important concerns in the neural tissue when illuminated with NIR light. Rodent models are frequently used to study laser-tissue interactions. As a part of ongoing research project in the neural interface laboratory, direct measurements of temperature in the rat brain cortex as a response to a pulsed sequence of NIR laser beam are available. In this thesis, finite element modeling approach is used to model and simulate the temperature elevation in neural tissue under the effect of NIR laser pulsing. Steady state and transient analyses are conducted, and spatio-temporal temperature maps are generated. The effect of pulse frequency is investigated. The results are compared with experimental data and found to be in good agreement. The finite element modeling allows studying various variables on the heating effect of NIR in neural tissue that would otherwise be very difficult to investigate experimentally.

FINITE ELEMENT MODELING OF TEMPERATURE ELEVATION DUE TO NIR EXPOSURE IN NEURAL TISSUE

by
Atabek Can Yucel

A Thesis
Submitted to the Faculty of
New Jersey Institute of Technology
in Partial Fulfillment of the Requirements for the Degree of
Master of Science in Biomedical Engineering

Department of Biomedical Engineering

May 2013

APPROVAL PAGE

FINITE ELEMENT MODELING OF TEMPERATURE ELEVATION DUE TO NIR EXPOSURE IN NEURAL TISSUE

Atabek Can Yucel

Dr. Mesut Sahin, Thesis Advisor — Date
Associate Professor of Biomedical Engineering, NJIT

Dr. Bryan J. Pfister, Committee Member — Date
Associate Professor of Biomedical Engineering, NJIT

Dr. Max Roman, Committee Member — Date
Assistant Research Professor of Biomedical Engineering, NJIT

Dr. Yahia M. Al-Smadi, Committee Member — Date
SR. Mechanical Engineer, AECOM

BIOGRAPHICAL SKETCH

Author: Atabek Can Yucel

Degree: Master of Science

Date: May 2013

Undergraduate and Graduate Education:

- Master of Science in Biomedical Engineering,
  New Jersey Institute of Technology, Newark, NJ, 2013

- Bachelor of Science in Electrical Engineering,
  Dokuz Eylul University, Izmir, Turkey, 2005

Major: Biomedical Engineering

I dedicate my work to my family, who has been a big support.

ACKNOWLEDGMENT

I would like to thank Dr. Mesut Sahin for his supervision, guidance and advice. Without his support, this study would have been much harder and taken longer time. I would also like to acknowledge Dr. Bryan J. Pfister, Dr. Max Roman and Dr. Yahia Al-Smadi for actively participating in the committee. I am grateful to Ammar Abdo and Ali Ersen for their cooperation and Dr. Jason Steffener for his support.

TABLE OF CONTENTS

Chapter	Page
1 INTRODUCTION……..……..…….	1
1.1 Objective …….....……..……...	1
1.2 Background Information …….……....	1
1.2.1 Absorption…….....	2
1.2.2 Scattering……	3
1.2.3 Laser Intensity Profile…….....	3
2 BIOHEAT TRANSFER……..	6
2.1 Introduction……..	6
2.2 Heat Transfer in Living Tissue……	6
3 FINITE ELEMENT ANALYSIS……	8
3.1 Introduction……..	8
3.2 Principles……..	8
3.3 Procedure……..	11
3.3.1 Pre Processing……	11
3.3.2 Analysis……..	11
3.3.3 Post Processing……...	11
4 METHODOLOGY……..	12
4.1 Surface Fitting Operation for the Laser Light Intensity Profile……...	12
4.2 Pre Processing……..	14

4.2.1 Defining the variables…… 14

4.2.2 Creating the geometry…… 17

4.2.3 Tissue parameters and the heat source……... 19

4.2.4 Creating mesh……. 21

4.2.5 Steady state and time dependent analysis parameters…… 22

4.3 Analysis…… 22

4.4 Post Processing……. 23

5 RESULTS……... 24

5.1 Fifteen Second Pulse Sequence at 100Hz…… 24

5.1.1 3D plots…….. 24

5.1.2 Temperature versus time plots……... 30

5.1.3 Heat Contours……. 37

5.2 Single Pulse…….. 45

6 DISCUSSION, CONCLUSION, AND FUTURE WORK…… 48

6.1 Results Comparison...……... 48

6.2 Temperature versus Time Plots…… 48

6.3 Single Pulse Plots……. 49

6.4 Temperature Distribution Plots…… 50

6.5 Conclusion……..... 51

6.6 Future Work……. 51

LIST OF TABLES

Table		Page
2.1	The variables used in the Pennes Bio-Heat equation……..	7
4.1	Light intensity values in the tissue……..	12
4.2	Tissue parameters that are entered into the FEA software……..	15

LIST OF FIGURES

Figure		Page
1.1	Light absorption in a medium…….	2
1.2	Light scattering in a medium……..	3
1.3	Laser intensity profile…….	4
3.1	Mesh structure for a 2D model created by the finite element analysis software…	9
3.2	Mesh structure for a 3D model created by the finite element analysis software…	10
4.1	Surface fitting operations in MATLAB……..	13
4.2	Pulse train created to be multiplied with the light intensity equation…….	15
4.3	Step function created to create on and off times of the heat source……	16
4.4	The rectangle created to define the region of interest…….	17
4.5	Region of interest and surrounding tissue……...	18
4.6	The model left after subtracting one half……	19
4.7	Defining parameters for the tissue to be used in the Pennes equation……	20
4.8	Mesh structure created by the software for the model……	22
5.1	Temperature distribution at t=0……..	25
5.2	Temperature distribution at t=0.1 seconds…….	26
5.3	Temperature distribution at t=1 second……..	27
5.4	Temperature distribution at t=3 seconds…….	28
5.5	Temperature distribution at t=7 seconds…….	28
5.6	Temperature distribution at t=15 seconds, at the end of the pulse sequence……..	29

5.7 Temperature versus time plot at x=0, y=0 under 15 second pulse sequence with 20% duty cycle…… 30

5.8 Temperature versus time plot at x=0, y=-500 under 15 second pulse sequence with 20% duty cycle…… 31

5.9 Temperature versus time plot at x=0, y=-1000 under 15 second pulse sequence with 20% duty cycle…… 32

5.10 Temperature versus time plot at x=0, y=0 under 15 second pulse sequence with 50% duty cycle…… 33

5.11 Temperature versus time plot at x=0, y=-200 under 15 second pulse sequence with 50% duty cycle…… 33

5.12 Temperature versus time plot at x=0, y=-500 under 15 second pulse sequence with 50% duty cycle…… 34

5.13 Temperature versus time plot at x=0, y=-1000 under 15 second pulse sequence with 50% duty cycle…… 34

5.14 Temperature versus time plot at x=300, y=0 under 15 second pulse sequence with 50% duty cycle…… 35

5.15 Temperature versus time plot at x=1000, y=-1000 under 15 second pulse sequence with 50% duty cycle…… 35

5.16 Temperature versus time plot at x=1000, y=-2000 under 15 second pulse sequence with 50% duty cycle…… 36

5.17 Temperature distribution at t=0……. 37

5.18 Temperature distribution at t=0.1……... 38

5.19 Temperature distribution at t=0.2……... 39

5.20 Temperature distribution at t=0.3……... 40

5.21 Temperature distribution at t=0.4……... 41

5.22 Temperature distribution at t=0.5……... 42

5.23 Temperature distribution at t=1…….. 43

5.24 Temperature distribution at t=2…….. 44

5.25 Cooling curves for 7 different points along x=0 axis after a 200 micro seconds single pulse…….. 45

5.26 Cooling curves for 7 different points along x=200 axis after a 200 micro seconds single pulse…… 46

5.27 Cooling curves for 7 different points along x=500 axis after a 200 micro seconds single pulse…… 47

CHAPTER 1

INTRODUCTION

1.1 Objective

The objective of this thesis is to simulate the temperature profile inside the rat brain while it is illuminated by a near infrared laser using the finite element method, and then compare the results with the experimental data for better understanding of the thermal effect of NIR irradiation in neural tissue. With computer modeling, some complex events such as the transient response to a step change in the heat source, and the heat propagation through the tissue can be investigated. After matching the simulation results to that of the experiments, individual parameters can be modified to study their effects which would not be possible in an experimental setup. This will provide a starting point for those in the field who want to investigate the thermal effect of near infrared lasers in neural tissue.

1.2 Background Information

Near infrared (NIR) lasers have been used in medical applications both for diagnosis and treatment purposes (Abdo, Ersen, & Sahin, 2011). One of the side effects of the light energy is the temperature increase in the tissue. During laser irradiation, the process of photon absorption and thermal energy diffusion in the targeted and surrounding tissue is crucial to understand (Crochet et al., 2006). The knowledge of the temperature elevation profile in tissue allows user to calibrate laser power, exposure time, laser distribution, and distance with safety.

While the photons travel through the tissue, besides getting absorbed, they also scatter. Absorption and scattering properties are dependent on the tissue type. Since these properties are directly related to the power absorption and the temperature increase in the tissue, they are important and they need to be determined carefully for any modeling application. NIR light between 700-900nm has minimal absorption and scattering (Gurnani, 2003).

1.2.1 Absorption

The absorption coefficient is a measure of the conversion of radiant energy to heat and chemical energy (Chylek, 1986). It is numerically equal to the fraction of energy absorbed from a light beam per unit of distance traveled in an absorbing medium.

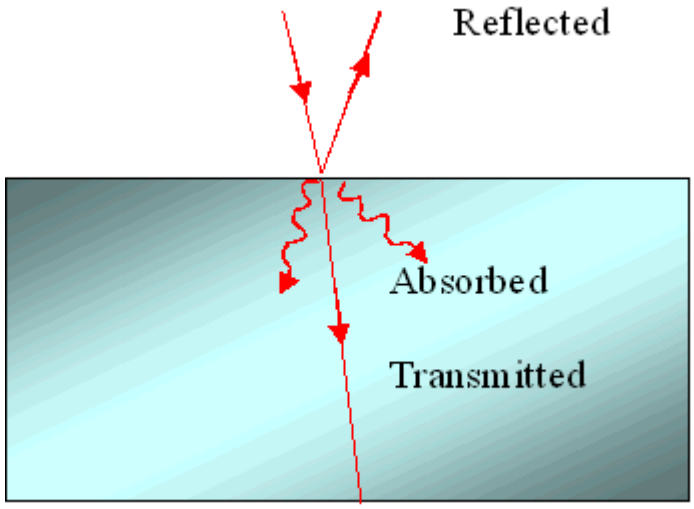

Figure 1.1 Light absorption in a medium

1.2.2 Scattering

The incident light scatters in all different directions. The scattering coefficient is equal to the fraction of energy dispersed from a light beam per unit distance traveled in a scattering medium (Bohren, 1983).

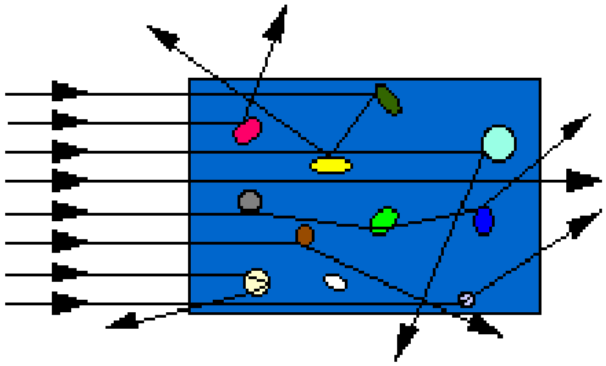

Figure 1.2 Light scattering in a medium

1.2.3 Laser Intensity Profile

The intensity profiles of the beam emitted by most lasers are Gaussian which defines the intensity change of the beam in its cross section. This type of profile has lower divergence than most other profiles. Low divergence allows the light to be transmitted to a longer distance without diverging, which is important for many applications, such as drilling.

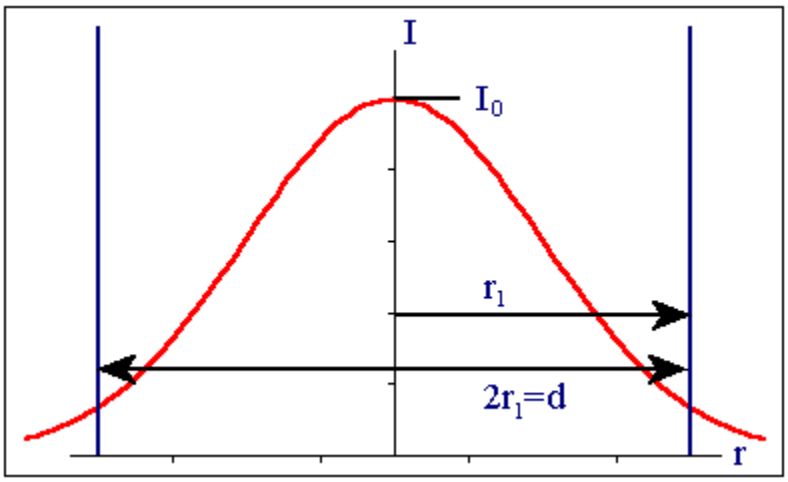

Figure 1.3 Gaussian intensity profile

The amplitude of the beam for a given point can be found using the equation,

$$E(r,z) = E_0 \frac{\omega_0}{\omega(z)} \exp\left(\frac{-r^2}{\omega^2} - ikz - ik\frac{r^2}{2R(z)} + i\varsigma(z)\right) \qquad (1.1)$$

where,

r is the radial distance from the center axis of the beam,

z is the axial distance from the beam's narrowest point,

i is the imaginary unit,

$k=2\pi/\lambda$ is the wave number,

$E_0 = |E(0,0)|$,

$\omega(z)$ is the radius at which the field amplitude and intensity drop to 1/e and $1/e^2$ of their axial values, respectively,

ω_0 is the waist size,

R(z) is the radius of curvature of the beam's wave fronts, and

$\varsigma(z)$ is the Gouy phase shift, an extra contribution to the phase that is seen in Gaussian beams.

The corresponding time-averaged intensity distribution is,

$$I(r,z) = I_0 \left(\frac{\omega_0}{\omega(z)}\right) exp\left(\frac{-2r^2}{\omega^2(z)}\right) \quad (1.2)$$

I_0 is the intensity at the center of the beam at its waist.

CHAPTER 2

BIOHEAT TRANSFER

2.1 Introduction

The topic of bio-heat transfer is becoming more important as new medical treatments that involve extreme temperatures are developed (Dewitt, 2002) . The most reliable and commonly used model is the Pennes bio-heat equation which is introduced by Harry H. Pennes as a modified version of heat equation to understand heat transfer in living tissues.

2.2 Heat Transfer in Living Tissue

Heat transfer in living tissue is a very complex mechanism which is influenced by blood perfusion, conduction, metabolism, and propagation. Tissue consists of solid, liquid, and gas and the characteristics of these materials change with the change in the temperature. In a living tissue, parameters change to keep the body temperature at a regulated level by adjusting the size of vessels (vasodilation) to adjust the amount of heat transfered more or less heat into the tissue from the blood, and also by sweating. There is an on-going research to model the bio-heat transfer in living tissue with better accuracy, but the Pennes equation is still considered satisfactory for many applications (Pennes, 1948).

$$\rho C \frac{\partial T}{\partial t} + \nabla(-k\nabla T) = \rho_b C_b \omega_b (T_b - T) + Q_{met} + Q_{ext} \tag{2.1}$$

Table 2.1 The variables used in the Pennes Bio-Heat equation

Variable	Explanation	Unit
ρ	Tissue density	kg/m^3
C	Specific heat of tissue	$J/(kg.K)$
K	Tissue thermal conductivity tensor	$W/(m.K)$
ρ_b	Blood density	kg/m^3
C_b	Specific heat of blood	$J/(kg.K)$
ω_b	Blood perfusion rate	$1/s$
T_b	Arterial blood temperature	K
Q_{met}	Metabolic heat source	W/m^3
Q_{ext}	Spatial heat source	W/m^3

.

CHAPTER 3

FINITE ELEMENT ANALYSIS

3.1 Introduction

With the growing technology, decision making for complex problems is becoming more dependent on approximate solutions made by computers. Finite element analysis (FEA) is one of the strongest computational techniques used for these approximate solutions. FEA has become commonplace in recent years, and is now the basis of a multibillion dollar industry (Roylance, 2001). FEA essentially cuts a structure into several pieces and connect the pieces with creating nodes, then solves simultaneous algebraic equations for each node to provide a solution for the whole system. This method is being used in a variety of fields. One of the important applications is to model bio-heat transfer. Common medical procedures like diagnosis, surgery, and prosthesis are known and visible but the biomechanical properties of tissues under these applications are not well known. Therefore, numerical modeling such as finite element approach has an important role determining unknown constitutive equations (Zhang, 2004).

3.2 Principles

For a single point with a single variable $\phi(x,y)$, a differential equation $P(x,y)$ can be satisfied with a mathematical solution. The same solution can be applied for multiple points, but in real life the problems usually involve complex geometries that cannot be calculated mathematically. For these practical problems, numerical calculations such as finite element analysis are used.

The essential point of the FEA is the mesh created by the method. This allows defining nodes on the structure that are somehow related to its neighbours. The method first determines solution for all of the nodes on the structure. For the points that are inside the meshes but not on the nodes, the results are interpolated by using the results calculated on the nodes.

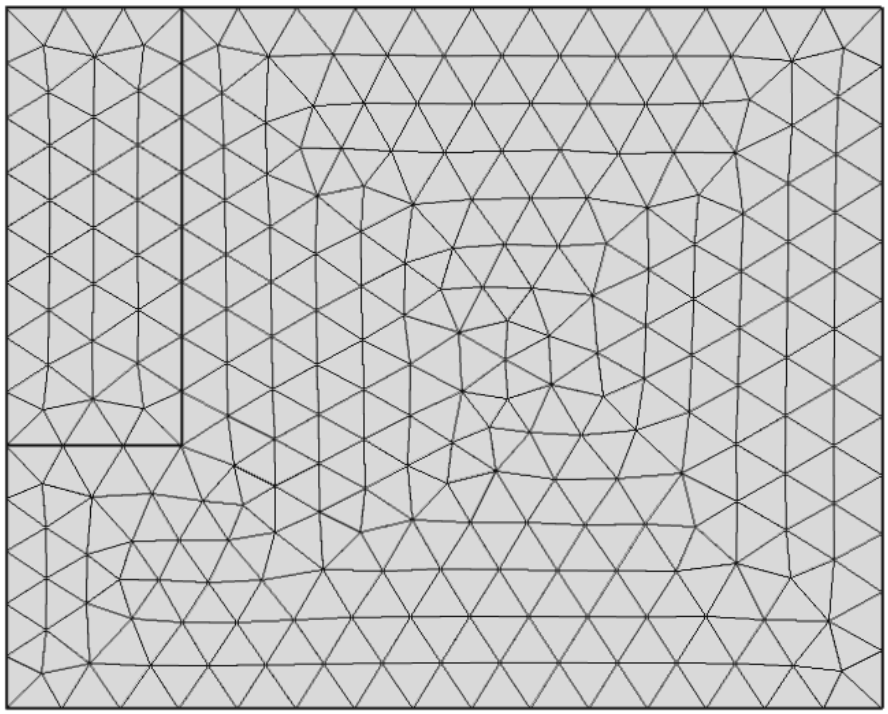

Figure 3.1 Mesh structure for a 2D model created by the finite element analysis software

For a triangular mesh any value in a triangle can be calculated from the three nodes using the equation.

$$\Phi(x,y)=N_1(x,y)\phi_1+ N_2(x,y)\phi_2+ N_3(x,y)\phi_3 \quad (3.1)$$

It can be concluded from the equation that the results from FEA is only estimations to the real values. A finer mesh means a better estimation, but it yields more nodes, and that means more calculations. Even with today`s advanced computers the calculation time is still an important aspect for complex structures. The tradeoff between time and better estimation is to be balanced depending on the application, since some applications require a better resolution, while others need to be fast.

For 3D applications, the same approach is used with more independent variables depending on the construction of the mesh generated.

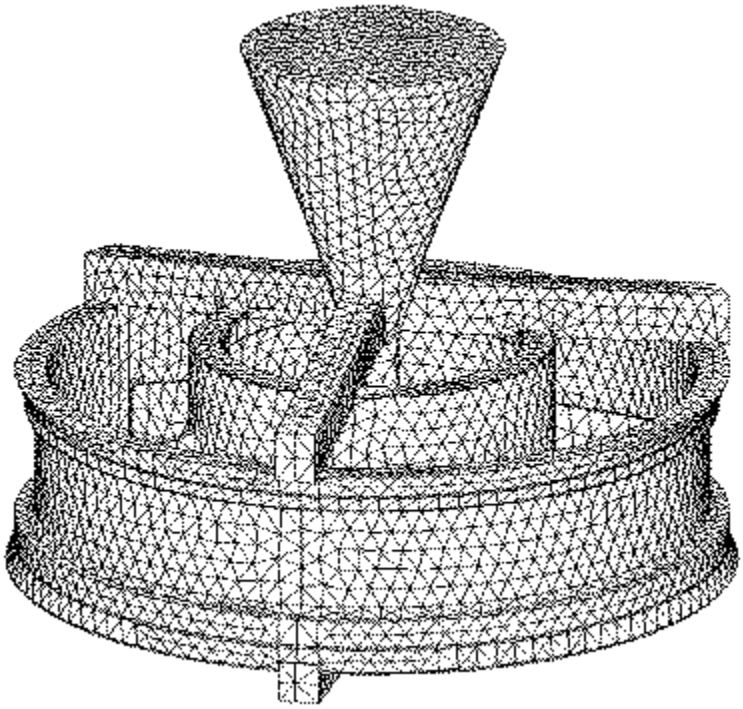

Figure 3.2 Mesh structure for a 3D model created by the finite element analysis software

3.3 Procedure

A finite element analysis is usually broken into three steps, which are embodied in most of the FEA software.

3.3.1. Pre Processing

At this step the user constructs the structure in the software or imports it from a CAD design, and defines the variables, material properties, and the equations used for the specific application. Since the method being used has a variety of fields, such as structure mechanics, fluids, heat transfer etc. the equations differs depending on the application. Most software has embedded equations for almost all of the applications. After the definitions, the structure is broken into pieces by creating a mesh. Then, the boundary conditions and loadings are defined.

3.3.2. Analysis

During the analysis phase, finite element software assembles the governing algebraic equations in matrix form and computes the unknown values (Hutton, 2004). These values are then used as base values for any additional computation.

3.3.3. Post Processing

Analysis and evaluation of the solution results are referred as post-processing which contains sophisticated routines for sorting, printing, and plotting selected results(Hutton, 2004). Depending on the application the outputs may vary, such as 2D or 3D plots, color-coded structural shapes or dynamic model behavior. In addition to these visual outputs, much FEA software includes functions to export the data to be used in other software.

CHAPTER 4

METHODOLOGY

4.1 Surface Fitting Operation for the Laser Light Intensity Profile

The main input for the project is the light distribution map created during the experiments. This map provides information about the light intensities at different locations in the tissue. It is not possible to use this map in the FEA software as a matrix. The data have to be entered as an analytic function involving two dimensions as the variables. Therefore, surface fitting on the data is necessary. To accomplish this task a matrix based engineering software, MATLAB, is used. The raw data show the light intensity in percentages at all locations in the model.

Table 4.1 Light intensity values in the tissue

y\x	0	50	100	200	300	400	500	600	700
0	100	91.41	71.63	27.98	8.267	2.666	0.678	0.138	0.052
-100	63.83	58.91	47.01	19.15	5.575	1.868	0.482	0.125	0.049
-200	43.62	39	29.57	11.26	3.363	1.167	0.263	0.104	0.045
-300	28.73	26.58	21.04	9.137	2.938	0.986	0.328	0.098	0.052
-400	18.51	17.16	13.78	6.504	2.403	0.891	0.275	0.101	0.061
-500	12.23	11.43	9.657	5.193	2.251	0.874	0.34	0.126	0.074
-700	8.674	8.154	6.882	3.881	1.843	0.685	0.288	0.144	0.088
-900	5.353	5.196	4.697	3.164	1.794	0.798	0.387	0.216	0.135
-1100	3.086	2.987	2.767	1.997	1.315	0.681	0.386	0.241	0.159
-1300	1.78	1.717	1.58	1.194	0.81	0.519	0.331	0.222	0.157
-1500	0.944	0.916	0.861	0.686	0.513	0.364	0.261	0.195	0.148
-1700	0.553	0.542	0.518	0.44	0.352	0.273	0.206	0.161	0.128
-1900	0.303	0.299	0.289	0.259	0.217	0.177	0.143	0.117	0.096
-2100	0.19	0.189	0.185	0.171	0.148	0.128	0.109	0.093	0.079
-2300	0.118	0.121	0.122	0.118	0.107	0.093	0.077	0.066	0.056
-2500	0.067	0.07	0.071	0.069	0.065	0.059	0.053	0.047	0.042

After entering the matrix into MATLAB, and converting them from percentages to real values, a curve fitting function ‘cftool’ is executed. On the interface, it is possible to use two vectors to define the normalized versions of X and Y locations for the points at which the measurements are taken, and a matrix for the measurement results at these locations. Since the characteristic of the data seems to be exponential, an exponential equation is entered. It is also possible to do a linear, cubic and bio harmonic fits with the built-in functions of the toolbox, but the best fit was achieved by a custom exponential equation.

Figure 4.1 shows the result of surface fitting operation with the black dots indicating the original data values and the color map showing the surface fit to the data points.

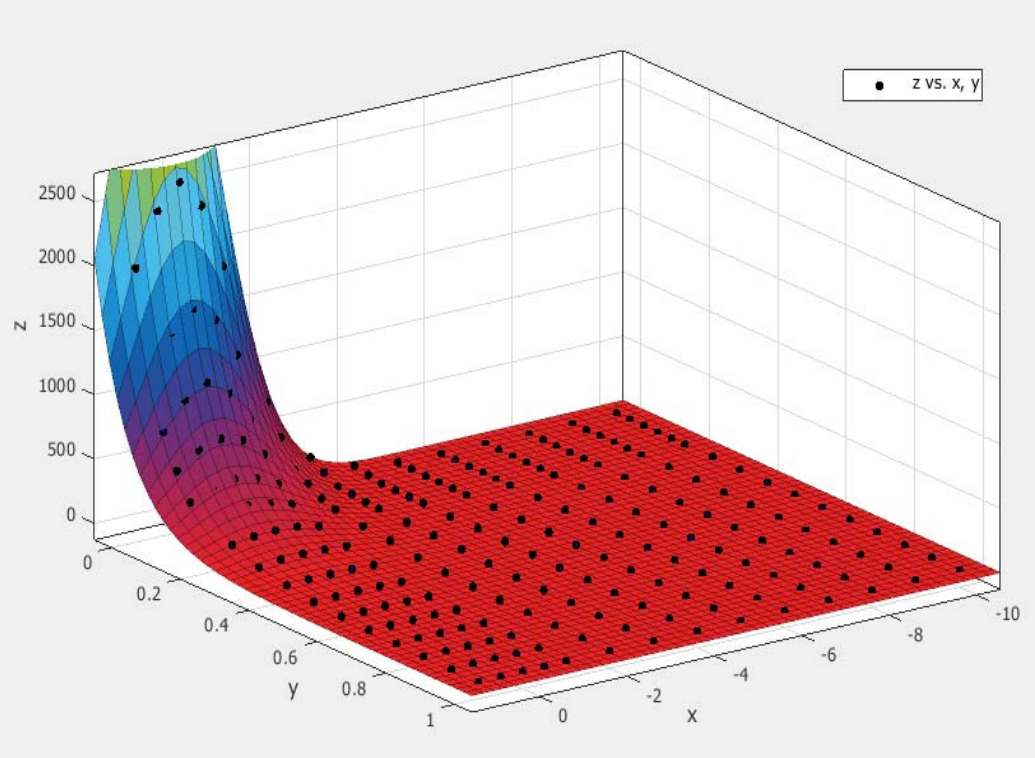

Figure 4.1 Surface fitting operations in MATLAB

Equation used for the surface fitting operation has three constants that are calculated by the MATLAB software.

$$Z = A.e^{\left(B.Y-(X^2/C)\right)} \tag{4.1}$$

The results taken from the toolbox then put into the equation as constants.

$$Z = 2541e^{\left(-10.23Y-(\frac{x^2}{3.307})\right)}(\frac{W}{cm^2}) \tag{4.2}$$

This equation is used as the heat source in the FEA model. The distribution then multiplied with the absorption coefficient (unit 1/cm) to calculate the power density (W/cm^3) for each data point.

4.2 Pre-Processing

4.2.1 Defining the variables

To start a model, first the parameters that are going to be used in the equations and the variables need to be defined. As indicated in the introduction, Pennes bio-heat equation is used for the model and the parameters for the equation are defined in the parameter section of the FEA software.

Table 4.2 Tissue parameters that are entered into the FEA software (Pryor, 2012)

Name	Expression	Value
rho_blood	1060[kg/m^3]	1060.0 kg/m³
C_blood	4200[J/(kg*K)]	4200.0 J/(kg·K)
T_blood	37[degC]	310.15 K
k_saline	0.2[W/(m*K)]	0.20000 W/(...
rho_saline	1200[kg/m^3]	1200.0 kg/m³
C_saline	3600[J/(kg*K)]	3600.0 J/(kg·K)
wb_saline	3e-3[1/s]	0.0030000 1/s
k_tissue	0.5[W/(m*K)]	0.50000 W/(...
rho_tissue	1050[kg/m^3]	1050.0 kg/m³
C_tissue	3600[J/(kg*K)]	3600.0 J/(kg·K)
wb_tissue	6e-3[1/s]	0.0060000 1/s
Q_met	400[W/m^3]	400.00 W/m³
T0	36.81[degC]	309.96 K
h_conv	.1[W/(m^2*K)]	0.10000 W/(...
T_inf	15[degC]	288.15 K

After defining the parameters, the equation of the heat source is entered, and a train of ones and zeros is defined that gets multiplied with the laser light intensity distribution profile to be able to apply the light as a pulse train or a single pulse. The pulse train is shown below.

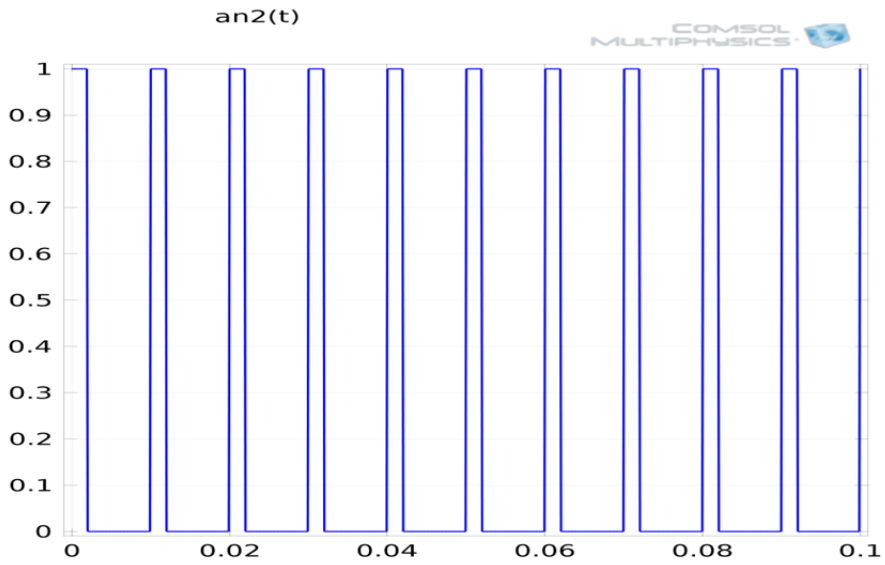

Figure 4.2 Pulse train to be multiplied with the light intensity equation.

A step function is defined also, because the laser should be off after a 15 second on period.

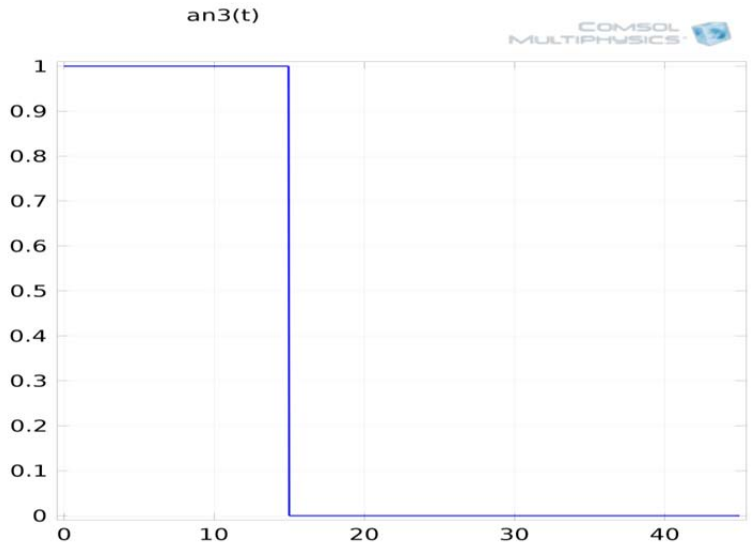

Figure 4.3 The step function that turns the laser on and off at times t=0 and t=15s respectively

4.2.2 Generating the Geometry

The experimental light intensity data that are used as the input were collected in a tissue volume of 1000 μm width and 2500 μm height. To define the heat source in a similar size of volume, a rectangle with these dimensions was generated. Since the measurements were taken in a 2D planar area within a 3D volume, the symmetry of the rectangle was also defined. During the analysis, the software extends the solution to 3D by using this symmetry option.

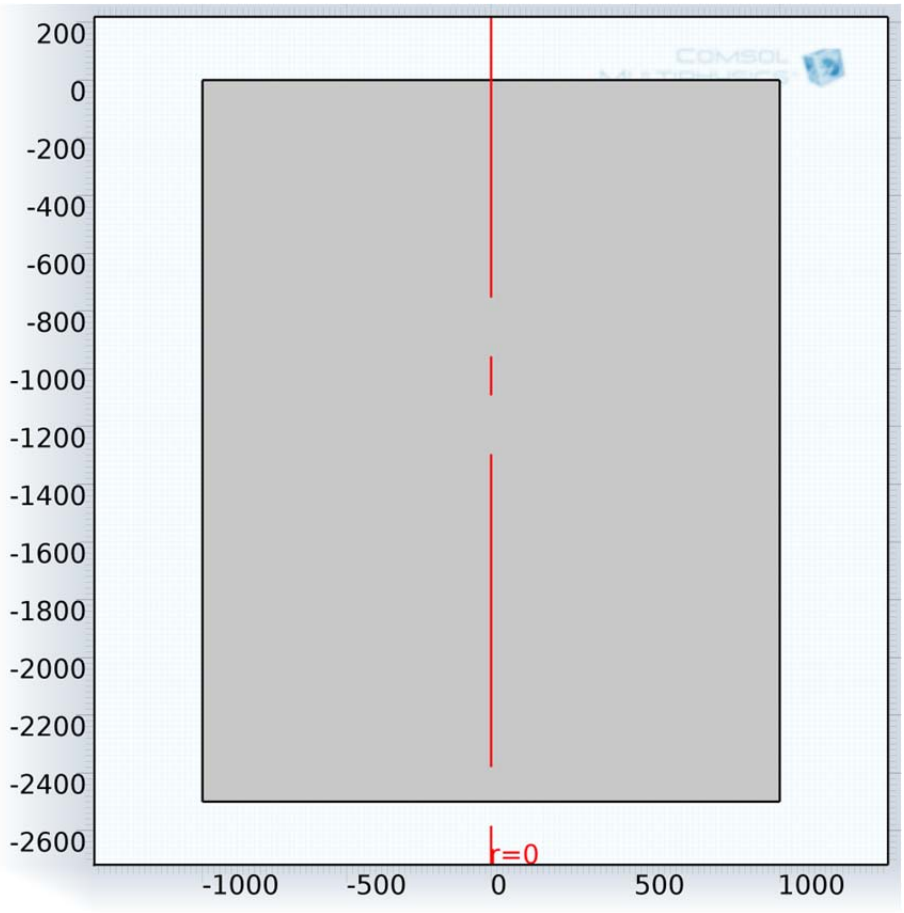

Figure 4.4 The rectangle that defines the region of interest in μm

The tissue surrounding the region of interest is also defined in the software. This is easier and more convenient than defining a boundary condition on the borders of the

region of interest. The surrounding tissue has to be much larger than the region of interest in order to minimize the error due to the boundary effects. Thus, another rectangle is created around the first one to model the rest of the brain tissue.

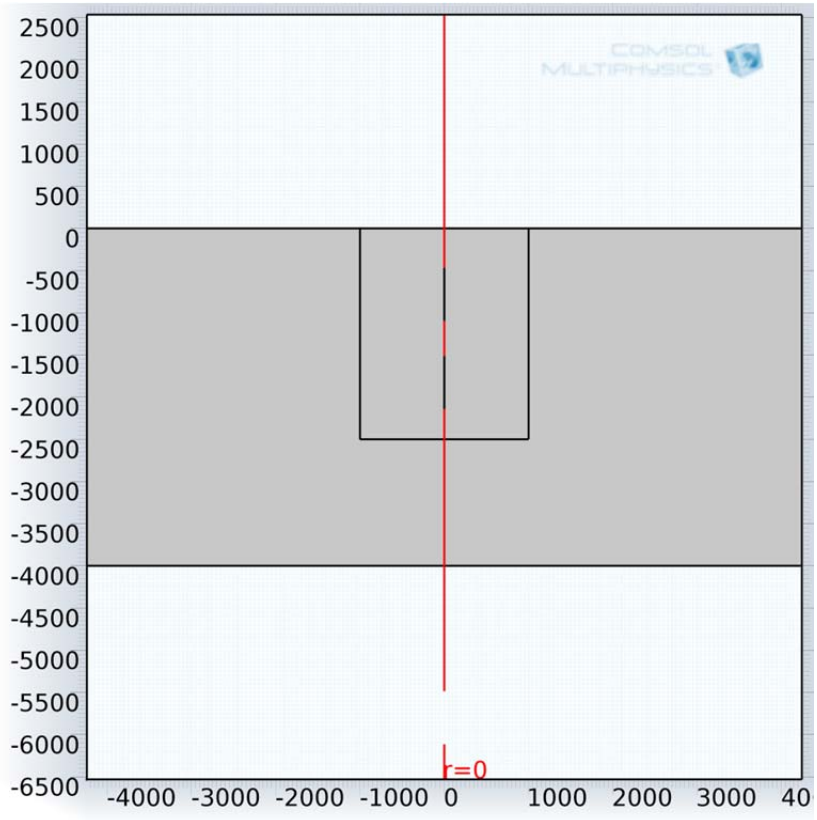

Figure 4.5 Region of interest and surrounding tissue in μm

Only one half of the region of interest is simulated because the results can easily be extrapolated to the whole volume by rotating the 2D half plane results along the center axis due to symmetry.

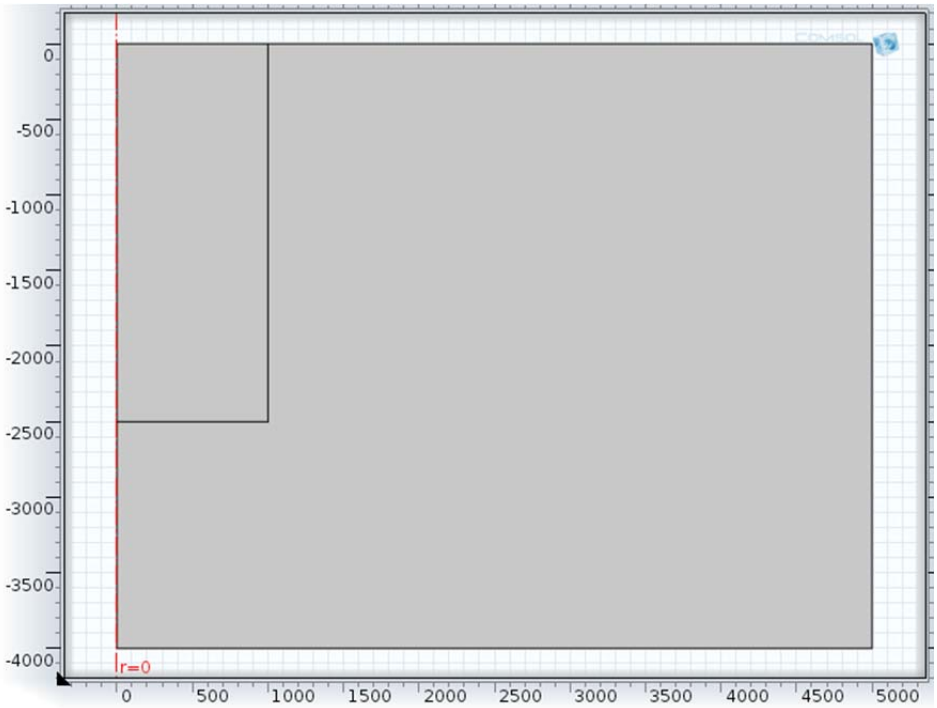

Figure 4.6 The model shown after cropping one half in μm

4.2.3 Tissue parameters and heat source

A single type of tissue is assumed for the entire volume, because the brain tissue that the measurements are taken from is mostly the gray matter and the thermal properties of white and gray matters are very similar. To define parameters the biological tissue function of the software is used. In this function, the heat equation is pre-defined and parameters can simply be entered as shown below in Fig. 4.7.

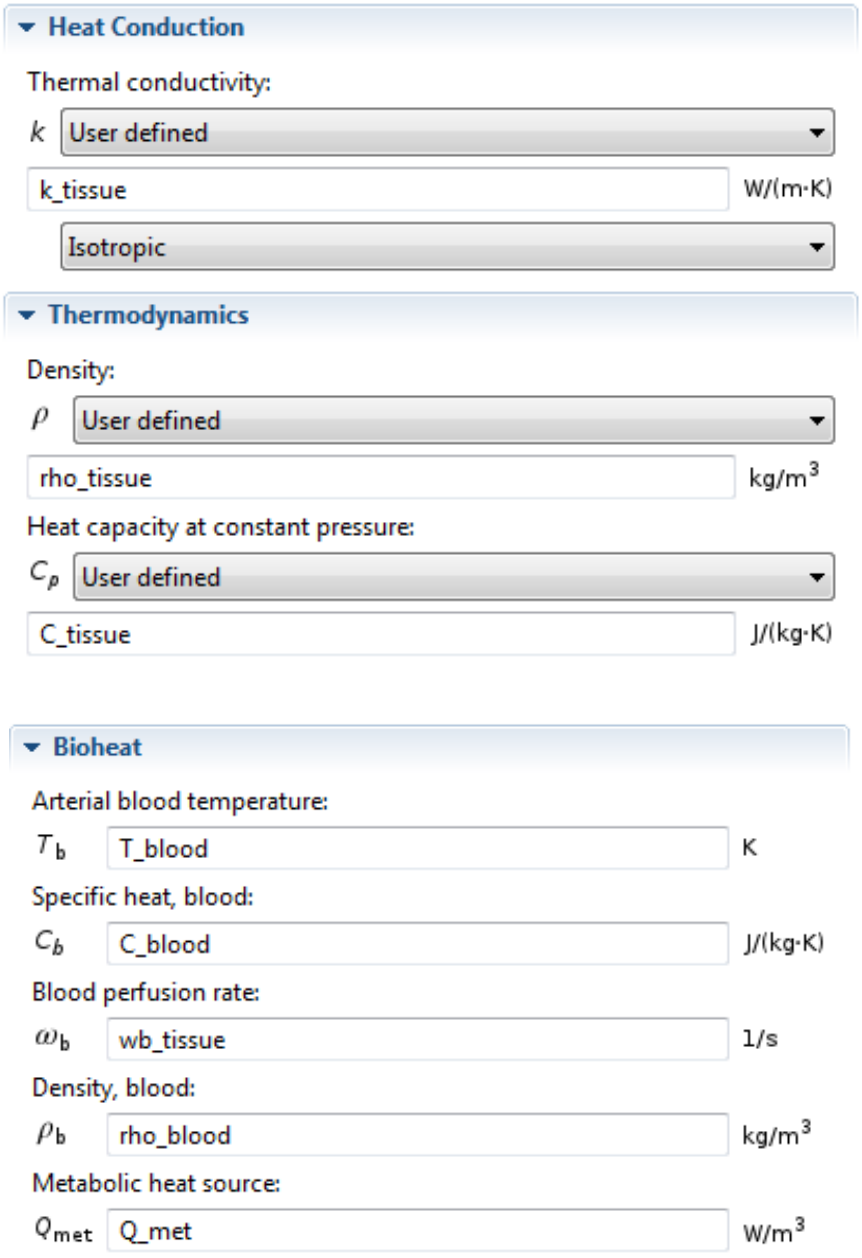

Figure 4.7 Entering tissue parameters in the Pennes equation

Next, the heat source is defined by entering the light distribution equation obtained in MATLAB, and multiplied with the absorption coefficient and the pulse train defined in the FEA software.

The last step of this part is to define a boundary condition for the surface of the tissue. As suggested by the experimental data, the heat loss from the surface into the pool of liquid over the cortex (as in the case of the animal experiments) is significant. Therefore, a convective cooling function is defined and the outside temperature is set to room temperature (COMSOL, 2012).

4.2.4 Creating Mesh

An important step of FEA is to create a mesh of the structure. The element size of the mesh depends on the project goals. If high accuracy is needed, the mesh should be fine, because that means creating more nodes and more points to calculate the values. On the other hand, if speed is more important, a coarser mesh can be used, which will reduce the number of nodes and the calculation time. For this project, two types of mesh density are used; a denser mesh for the region of interest, and a coarser one for the surrounding brain tissue.

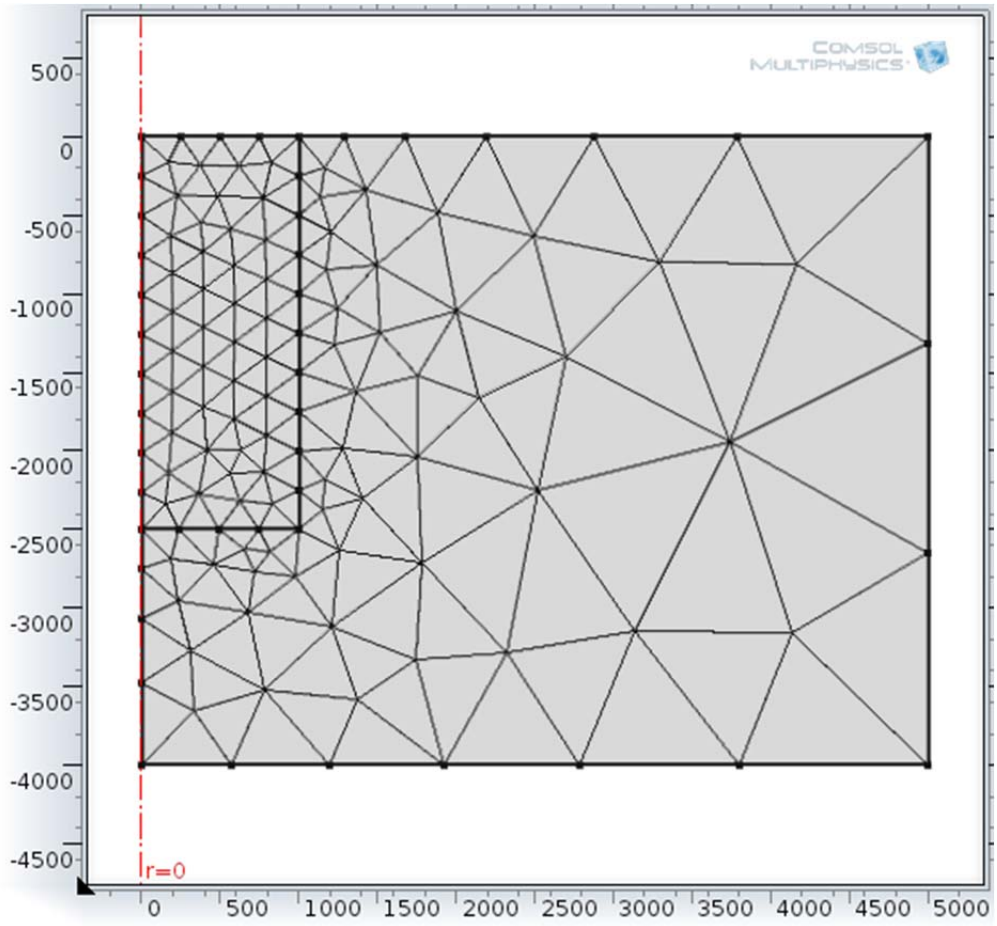

Figure 4.8 Mesh, created by the software, fine for the region of interest and coarse for the surrounding tissue in μm.

4.2.5 Steady state and time dependent analysis parameters

The last part of the preprocessing is to define parameters for the analysis. In this project, there are two processing steps. First study is to analyze the tissue without the heat source to find a baseline where all the temperatures are at equilibrium. During this time, there is a significant heat exchange and the software runs the model until temperature gradient is zero.

Second step is the transient analysis. The parameters entered for this part is the start and finish times and the step size. The software basically calculates the temperature at every node for every time point and uses the outputs of the previous time point as the initial condition for the next one. These parameters directly affect the calculation time, thus different time intervals and step sizes are used for different runs depending on the particularaim of the simulation.

4.3 Post Processing

The software is capable of providing various types of outputs such as plots, data sets, graphs etc. The results are presented in the next chapter.

CHAPTER 5

RESULTS

5.1 Fifteen Second Pulse Sequence at 100 Hz

The first set of results was taken under 15 second pulse train at 100 Hz with 20% duty cycle. Second set of result was recorded under a 15 second pulse train at 50 Hz and 50% duty cycle.

5.1.1 3D Plots

3D views of the temperature distribution were generated by the software by rotating the 2D model around the center axis. These graphs show the temperature value at every point for a specific time for the first pulse train. First, the view at t=0 is plotted to observe the temperature distribution just before the heat source is applied.

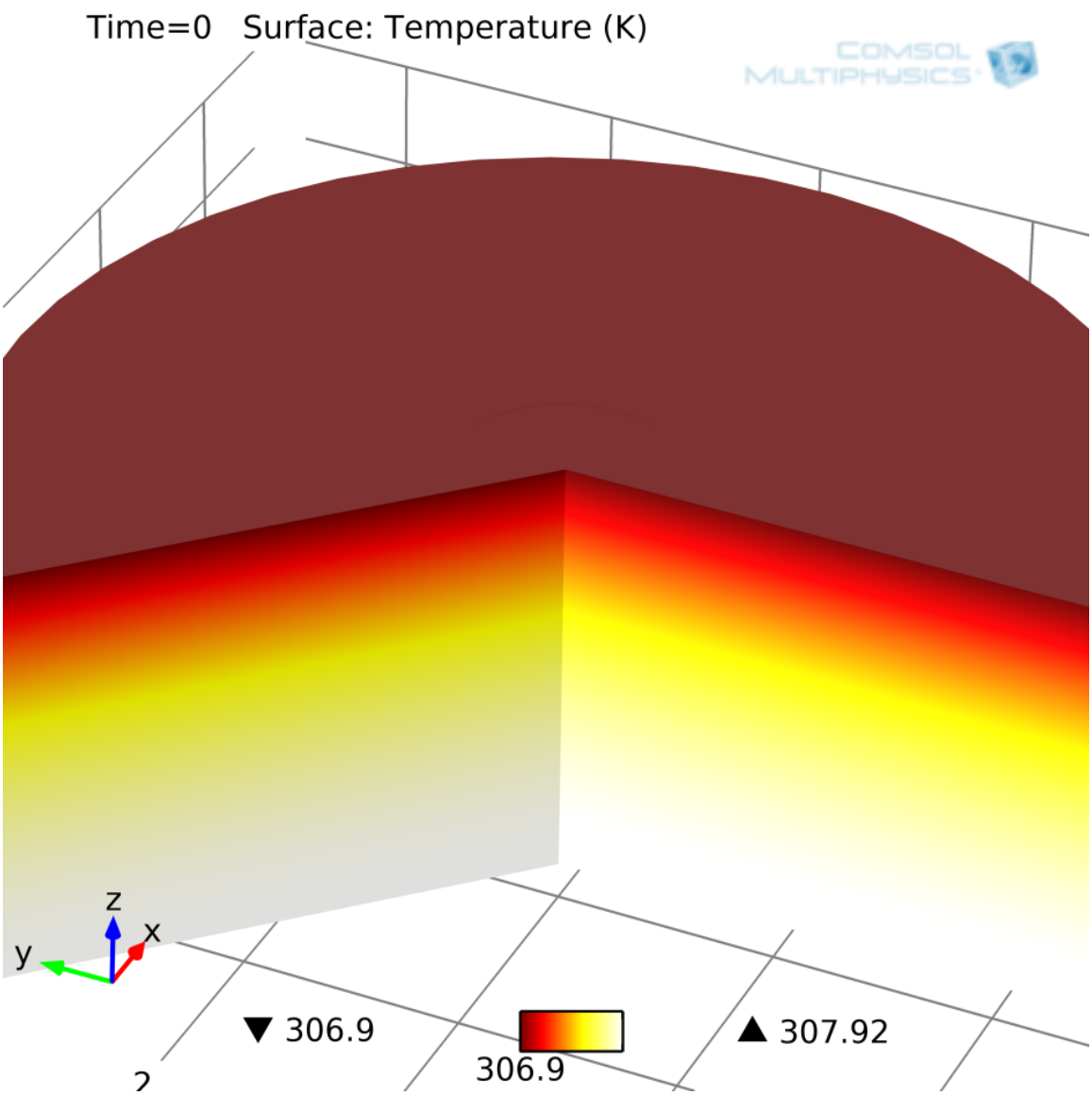

Figure 5.1 Temperature distribution at t=0

The surface temperature is lower than deeper parts of the tissue due to the heat loss on the surface. After the laser application there is a rapid increase in temperature in the areas that are closest to the NIR laser.

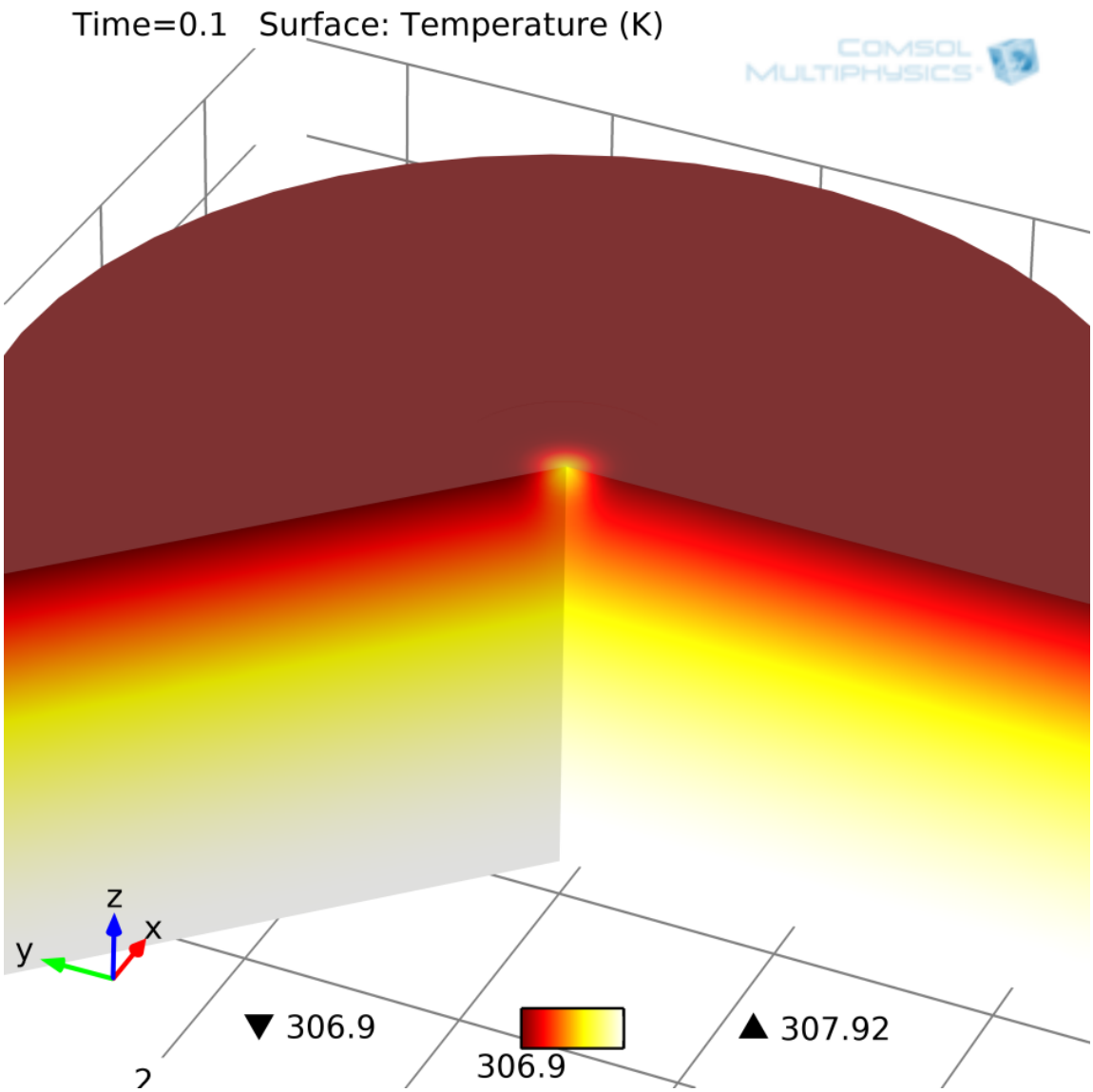

Figure 5.2 Temperature distribution at t=0.1 seconds

The heat propagates through the tissue as a function of time and the effect of the heat source becomes increasingly more obvious.

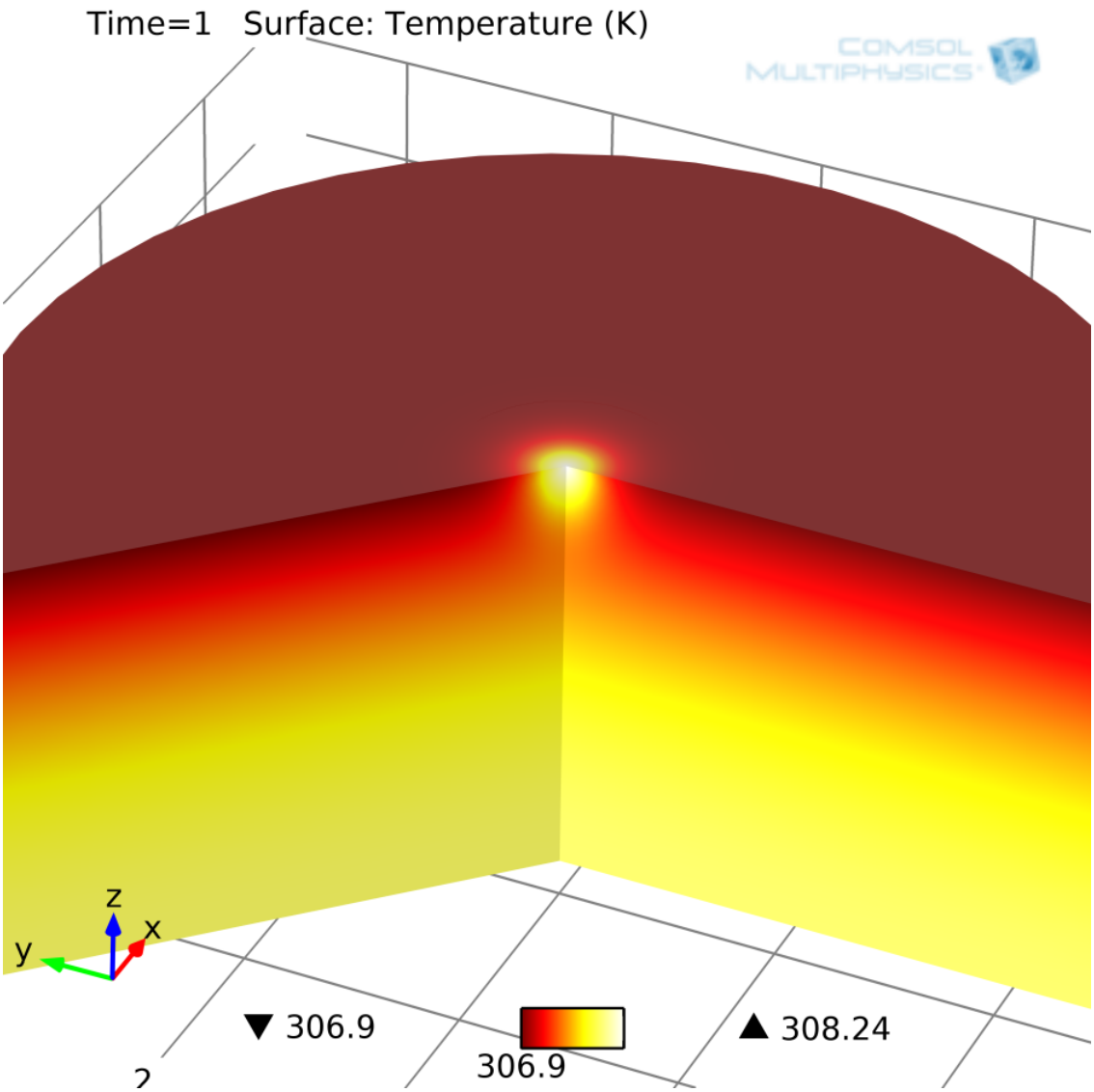

Figure 5.3 Temperature distribution at t=1 second

After a certain time point, the rate of temperature increase becomes much smaller than that of the initial 3-4 seconds of the laser application, as the system is approaching the steady state.

Figures 5.4 5.5 and 5.6 show the temperature distribution for t=3, t=7 and t=15.

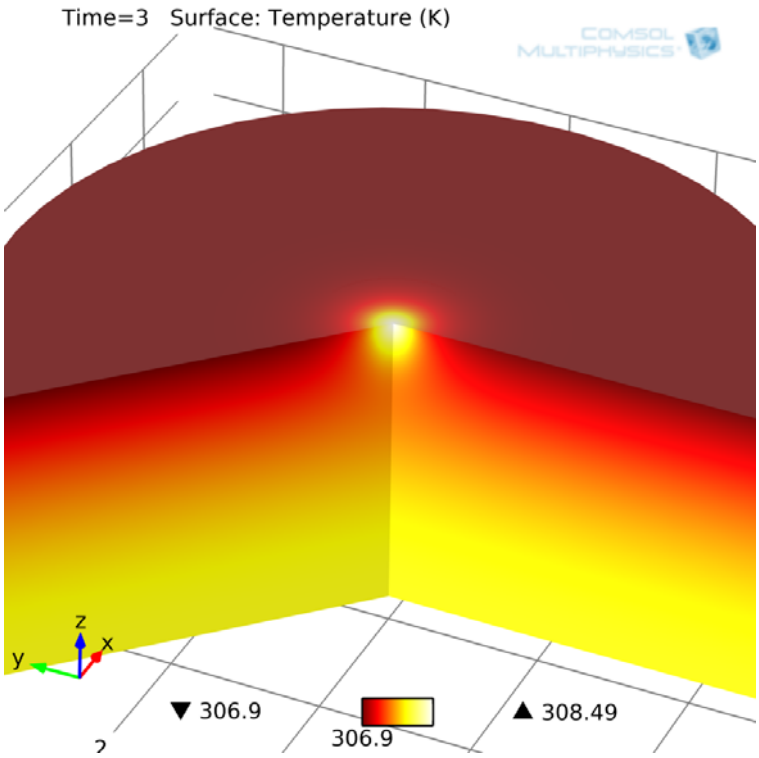

Figure 5.4 Temperature distribution at t=3 seconds

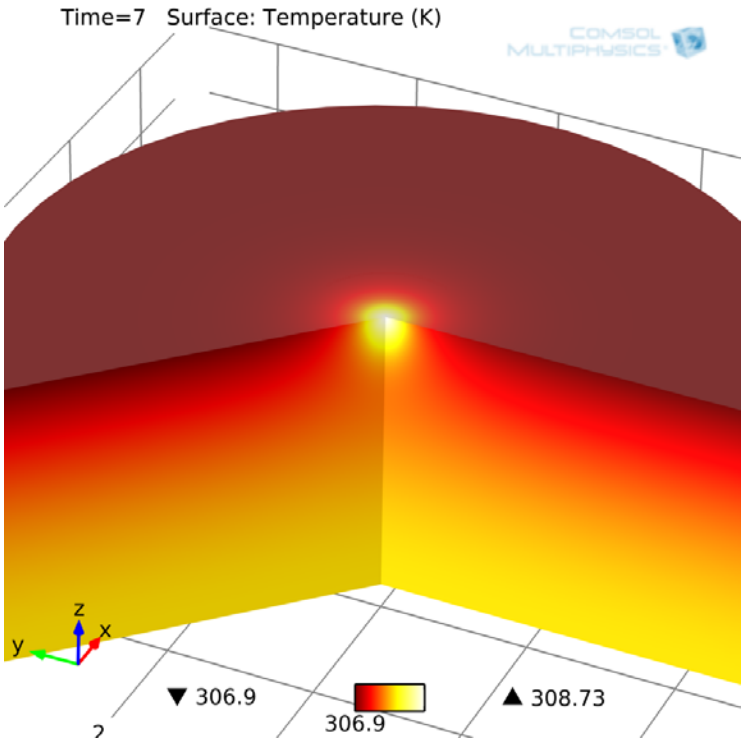

Figure 5.5 Temperature distribution at t=7 seconds

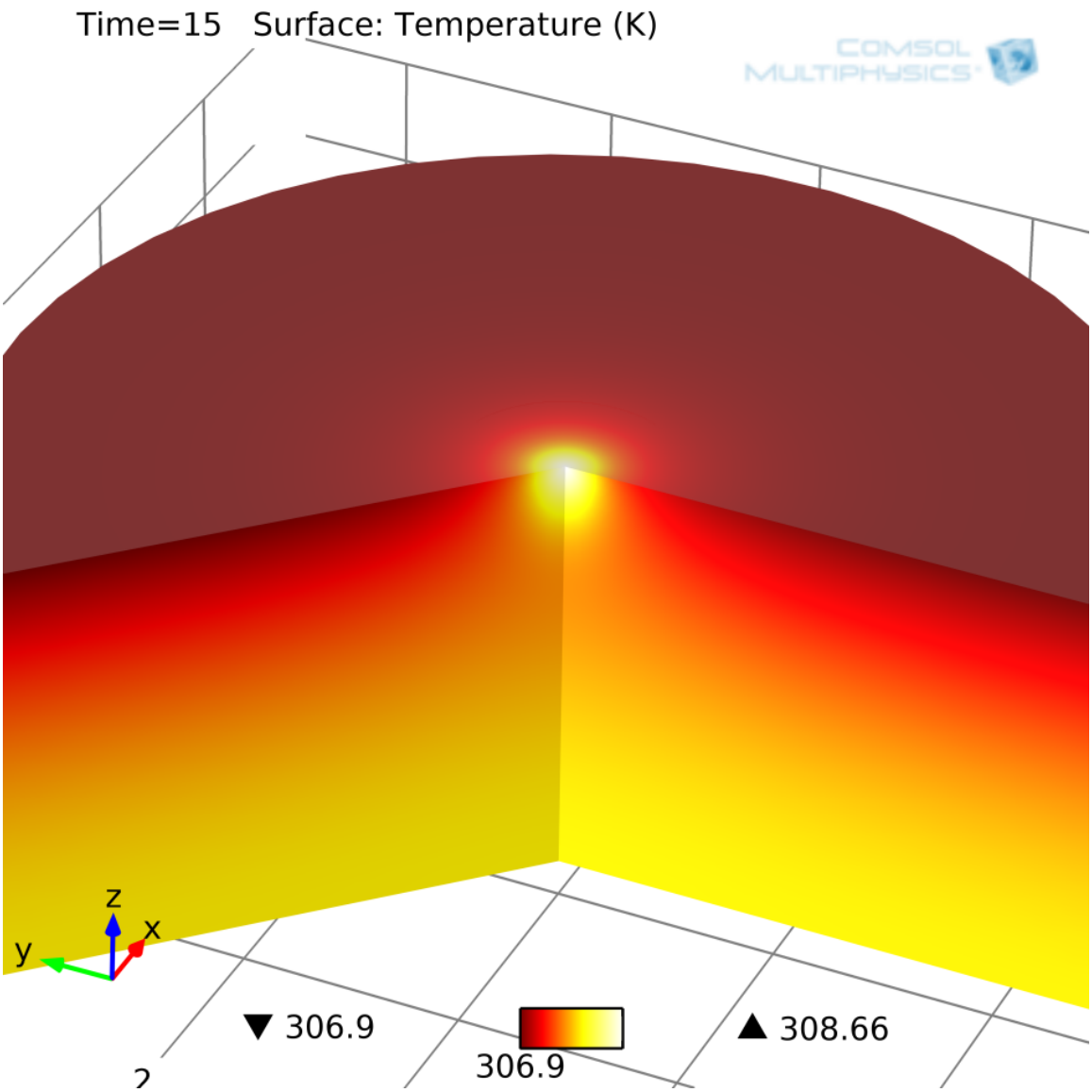

Figure 5.6 Temperature distribution at t=15 seconds, at the end of the pulse sequence.

5.1.2 Temporal plots of temperature

These plots show the temperature values versus time for a specific point in the tissue volume. These are used to compare the temperature values and the time constants for different points in the tissue. The plots were made for both pulse trains to show the difference in the temperature increase characteristics of the same points under different pulse trains. The first plot shows the temperature at the point that is closest to the heat source in the center.

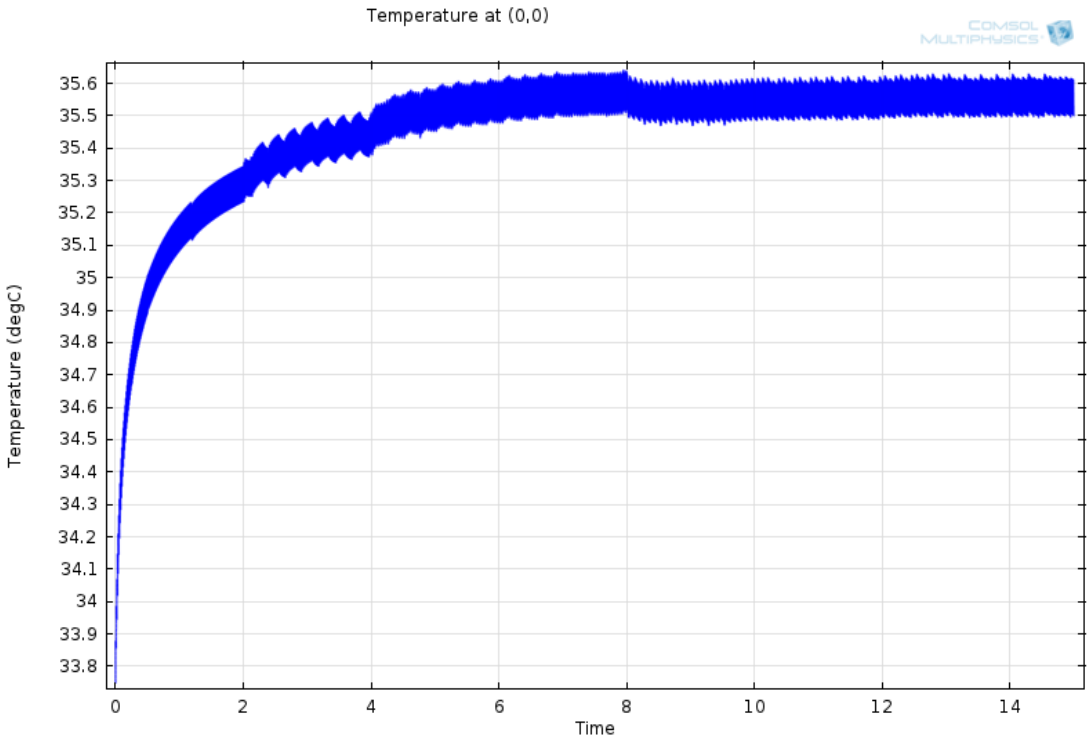

Figure 5.7 Temperature versus time plot at x=0, y=0 under 15 second pulse sequence with 20% duty cycle

The temperature values for the second plot are taken from a deeper region in the tissue. This means that the point is far from the heat source compared to the previous plot, so the difference between maximum and minimum temperature values is smaller.

The second pulse train results a temperature increase that is higher than the first pulse train. The temperature characteristics of the tissue under the effect of the second pulse train are shown below in Figures 5.10 through 5.16.

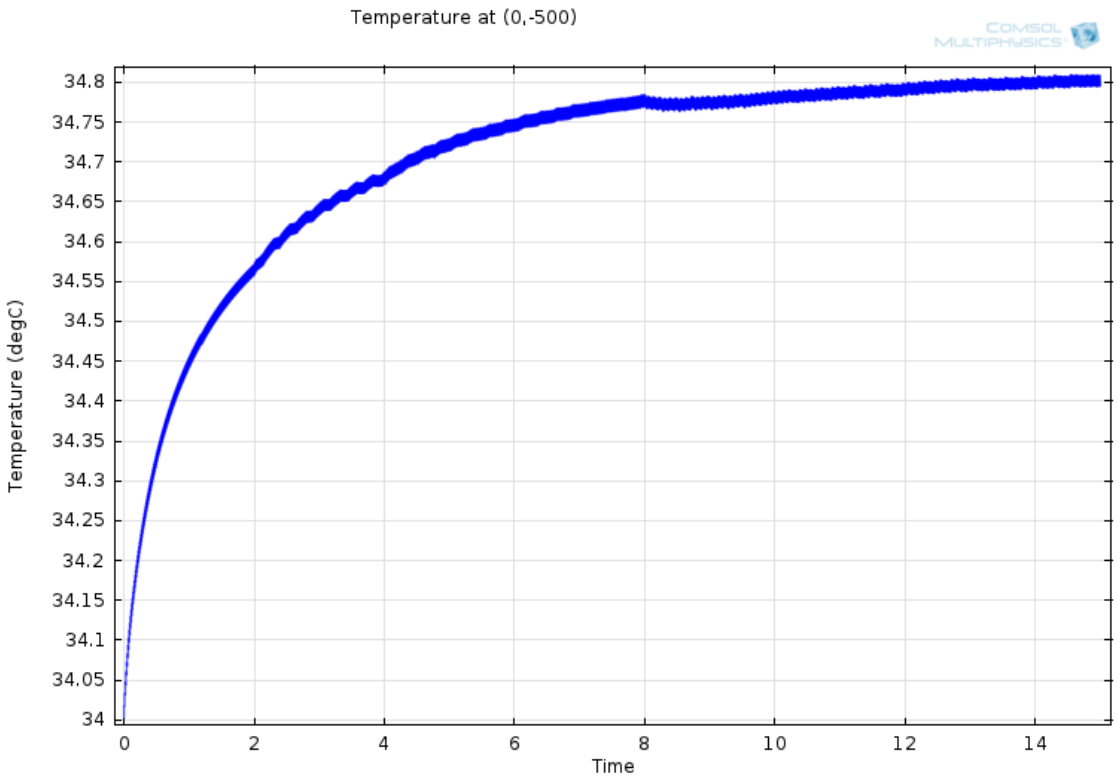

Figure 5.8 Temperature (^{o}C) versus time (s) plot at x=0, y=-500 under 15 second pulse sequence with 20% duty cycle

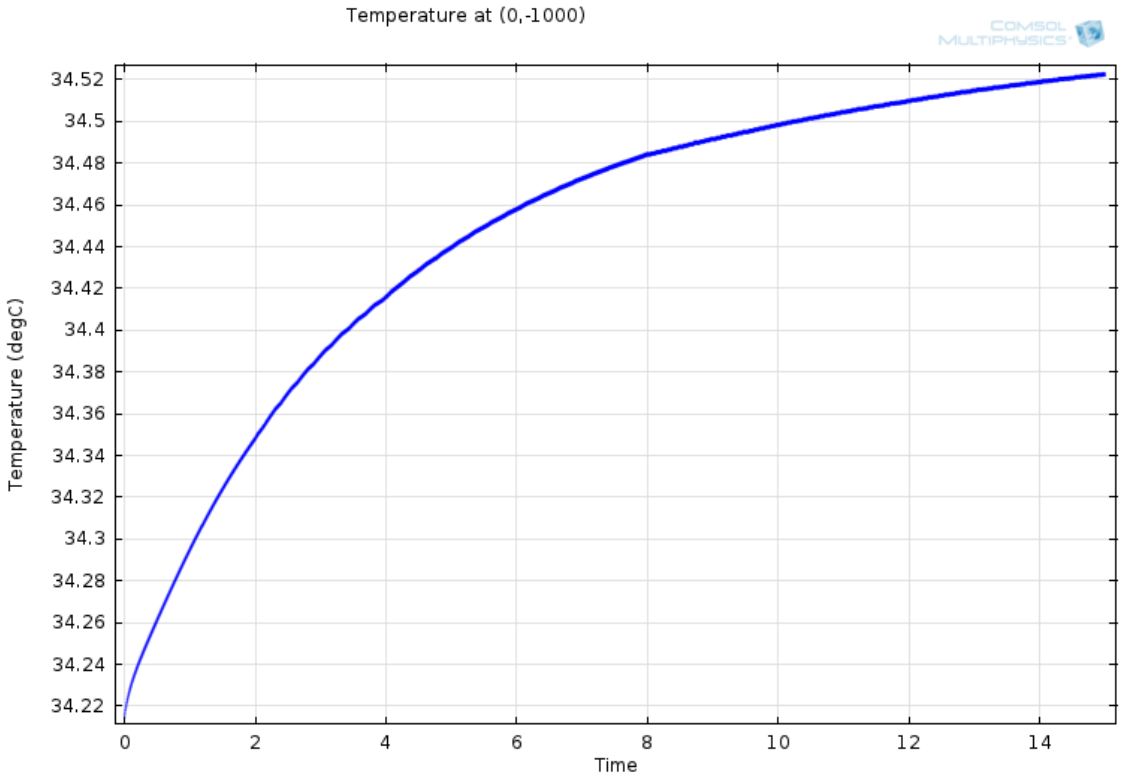

Figure 5.9 Temperature (^{o}C) versus time (s) plot at x=0, y=-1000 under 15 second pulse sequence with 20% duty cycle

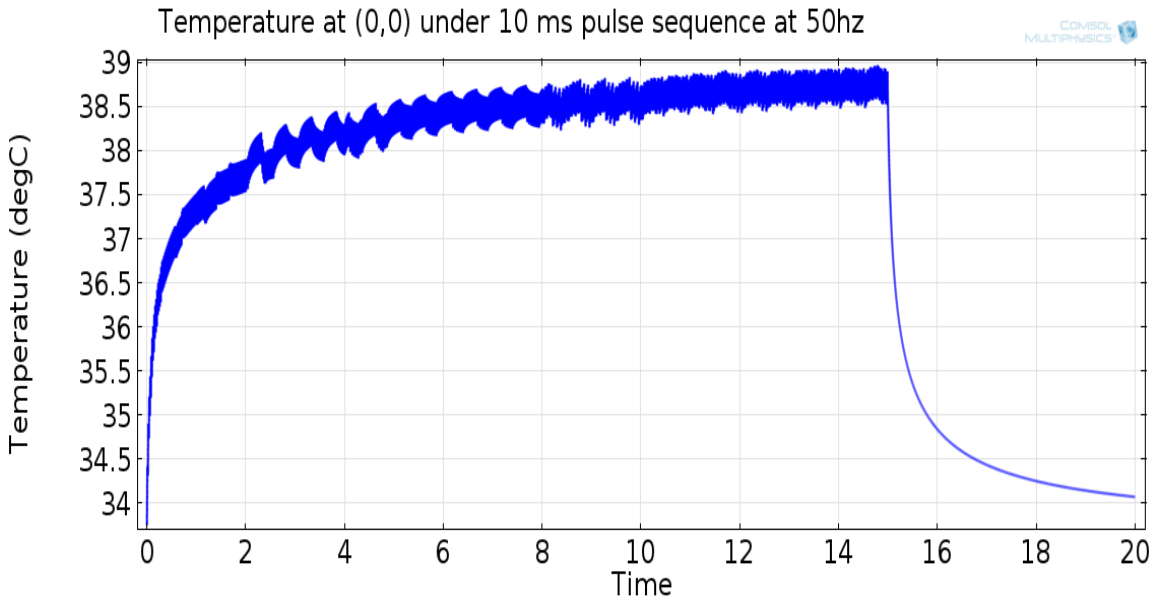

Figure 5.10 Temperature (^{o}C) versus time (s) plot at x=0, y=0 under 15 second pulse sequence with 50% duty cycle

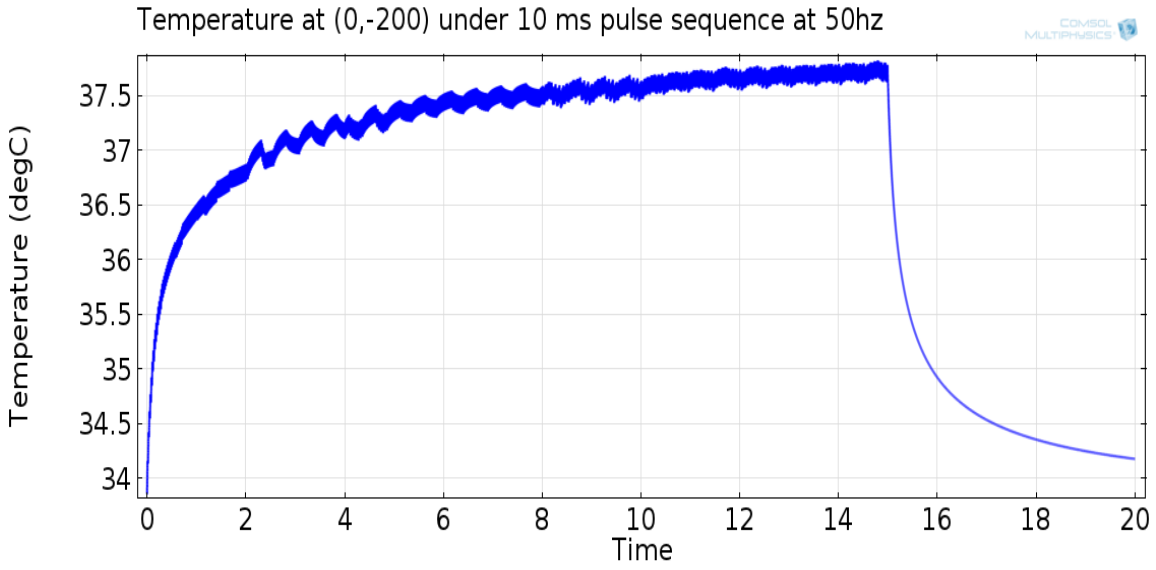

Figure 5.11 Temperature (^{o}C) versus time (s) plot at x=0, y=-200 under 15 second pulse sequence with 50% duty cycle

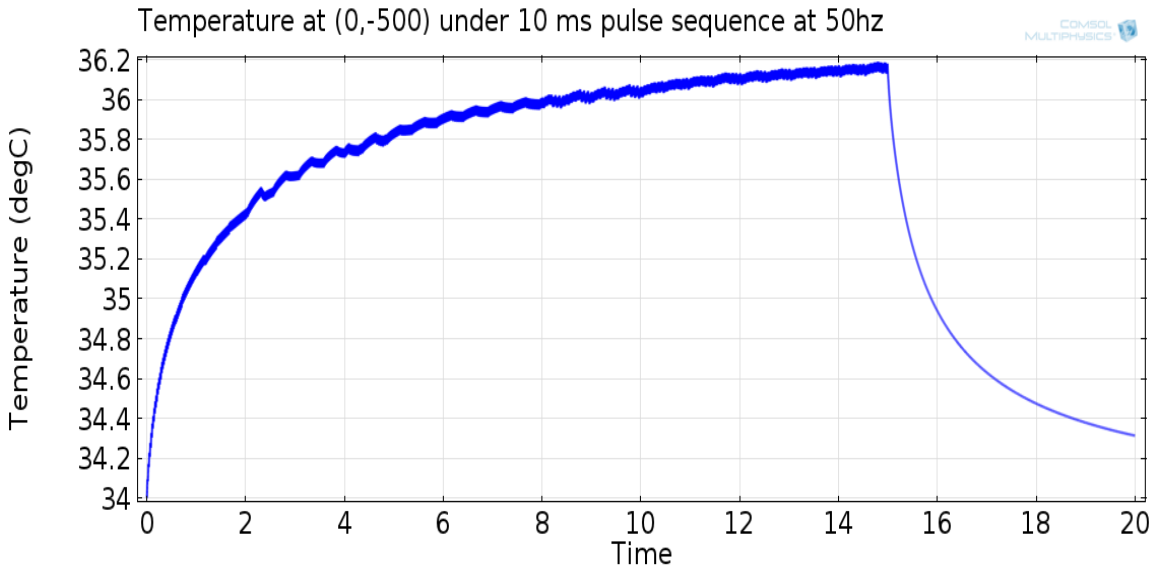

Figure 5.12 Temperature (^{o}C) versus time (s) plot at x=0, y=-500 under 15 second pulse sequence with 50% duty cycle

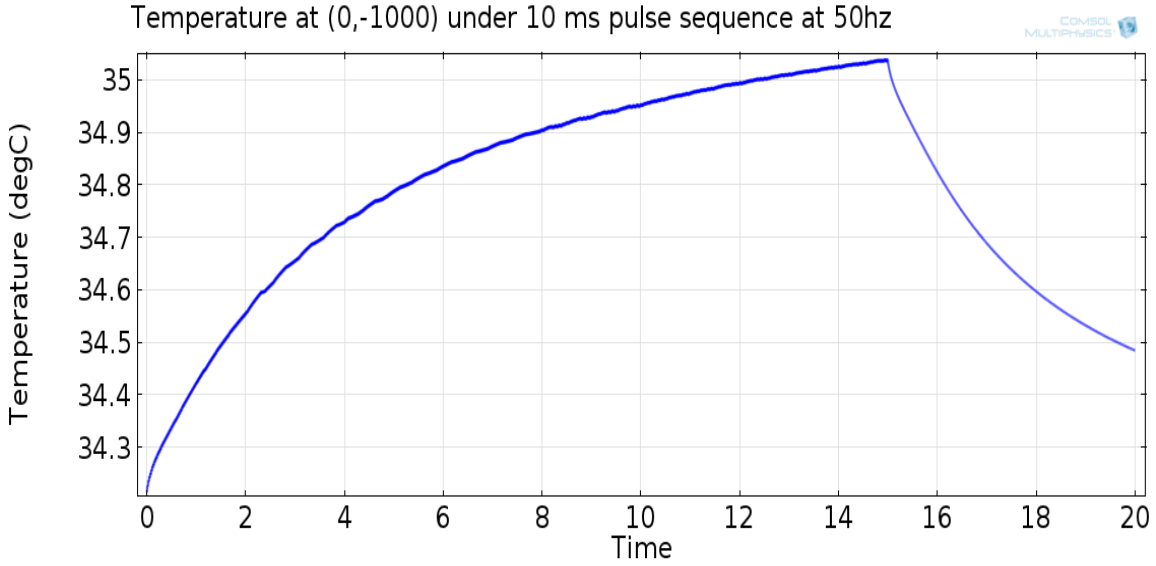

Figure 5.13 Temperature (^{o}C) versus time (s) plot at x=0, y=-1000 under 15 second pulse sequence with 50% duty cycle

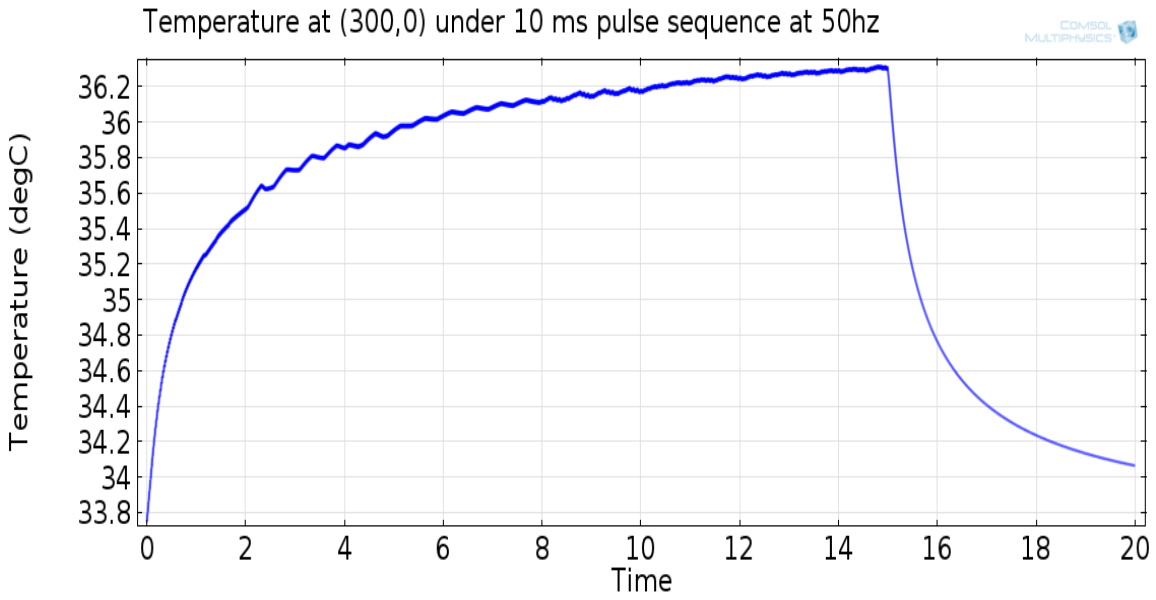

Figure 5.14 Temperature (^{o}C) versus time (s) plot at x=300, y=0 under 15 second pulse sequence with 50% duty cycle

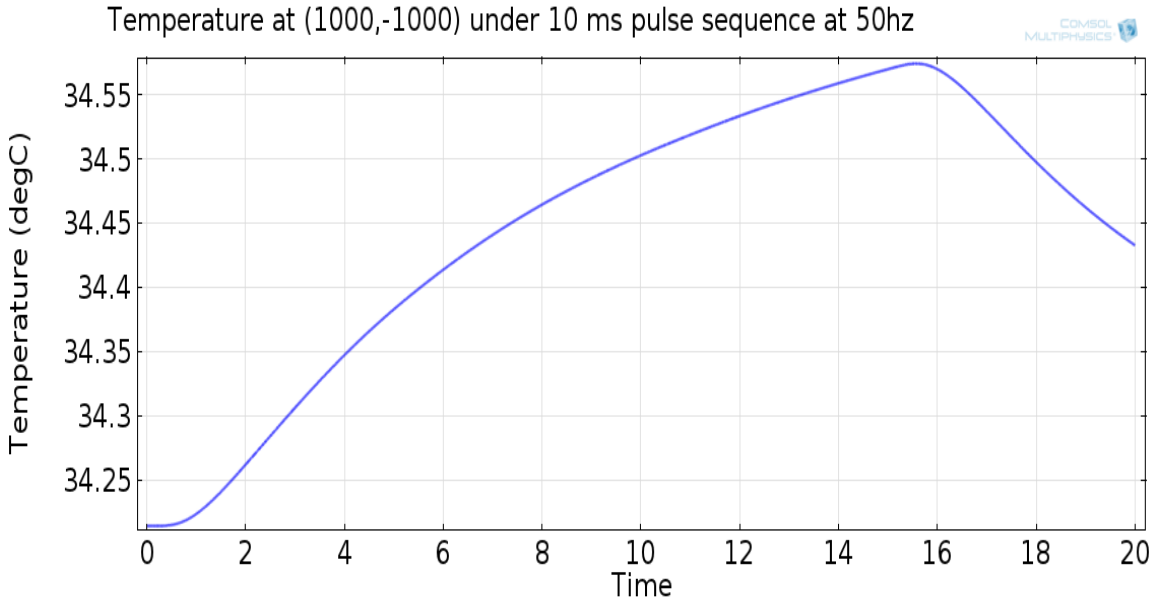

Figure 5.15 Temperature (^{o}C) versus time (s) plot at x=1000, y=-1000 under 15 second pulse sequence with 50% duty cycle

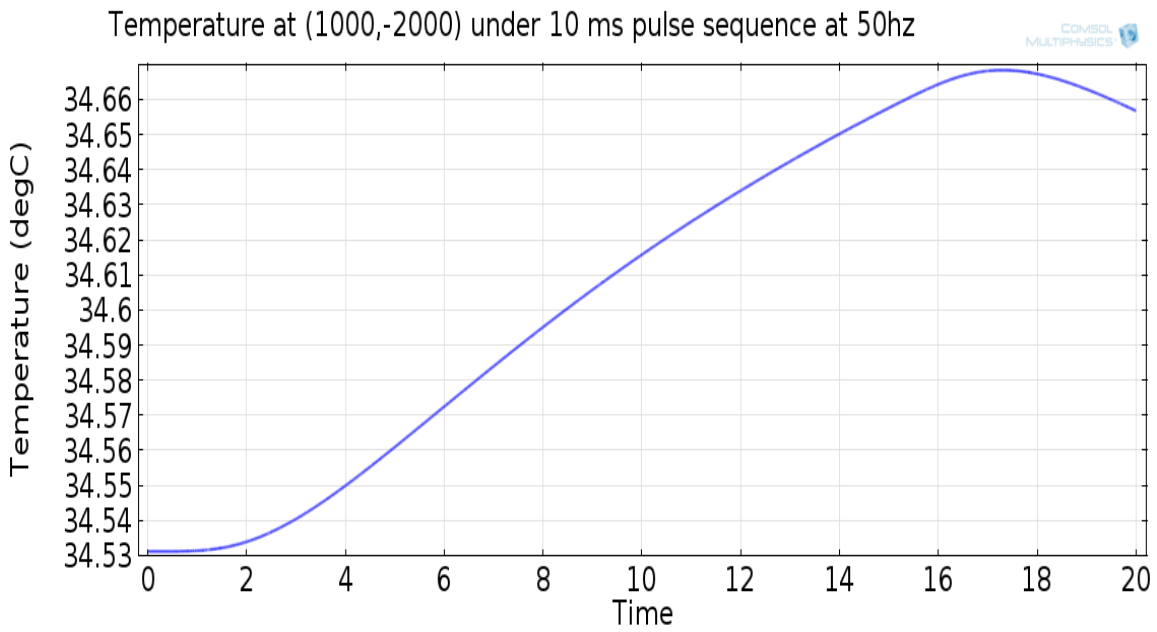

Figure 5.16 Temperature (^{o}C) versus time (s) plot at x=1000, y=-2000 under 15 second pulse sequence with 50% duty cycle

5.1.3 Heat contours

To observe the heat propagation in the tissue; the temperature distribution is examined at different time points.

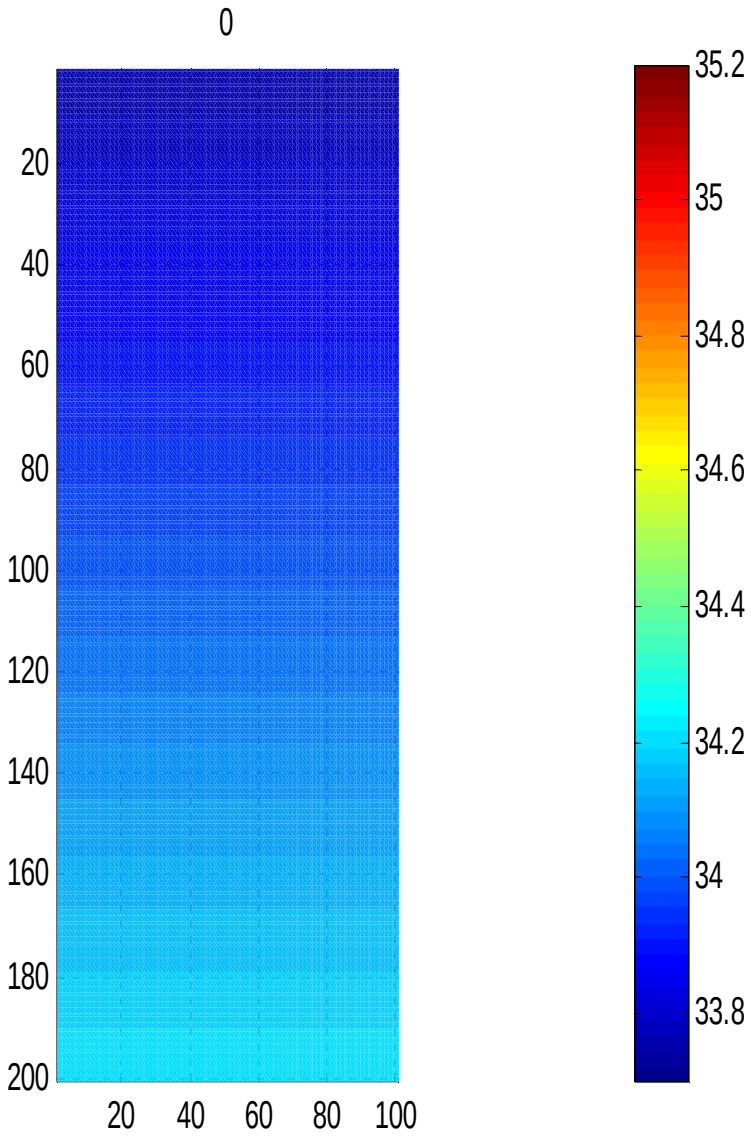

Figure 5.17 Temperature distribution at t=0 s

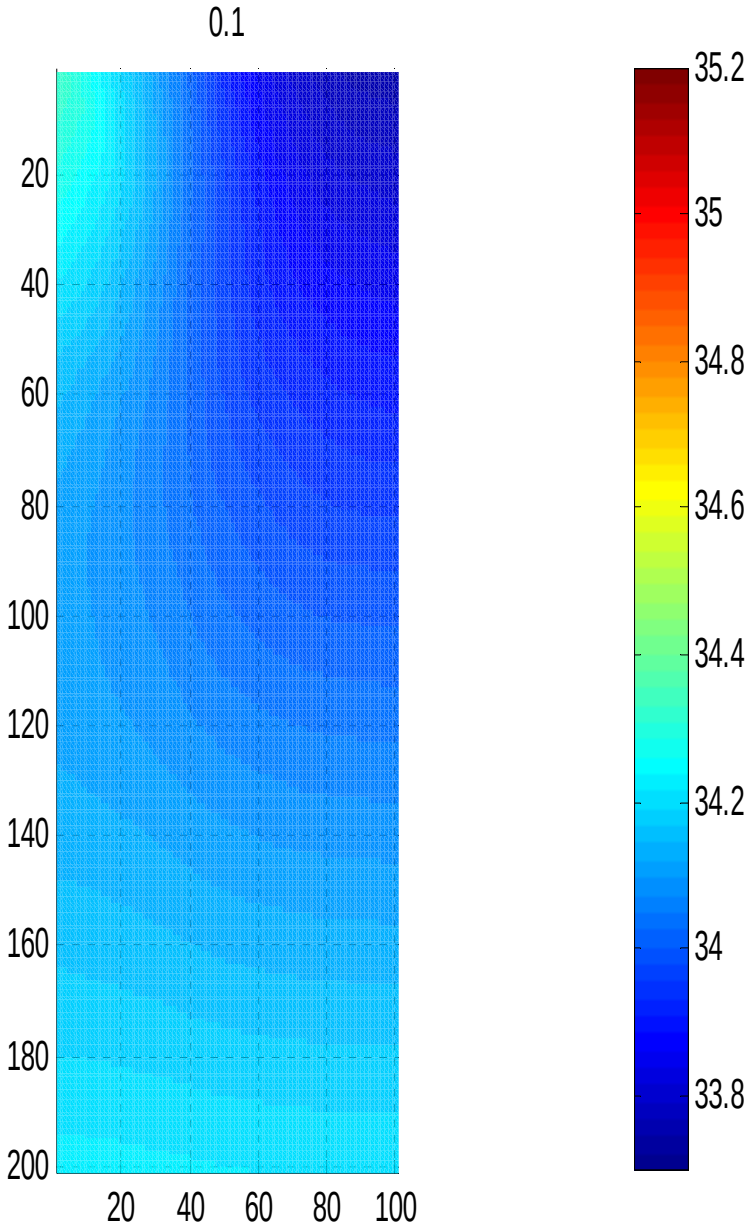

Figure 5.19 Temperature distribution at t=0.1 s

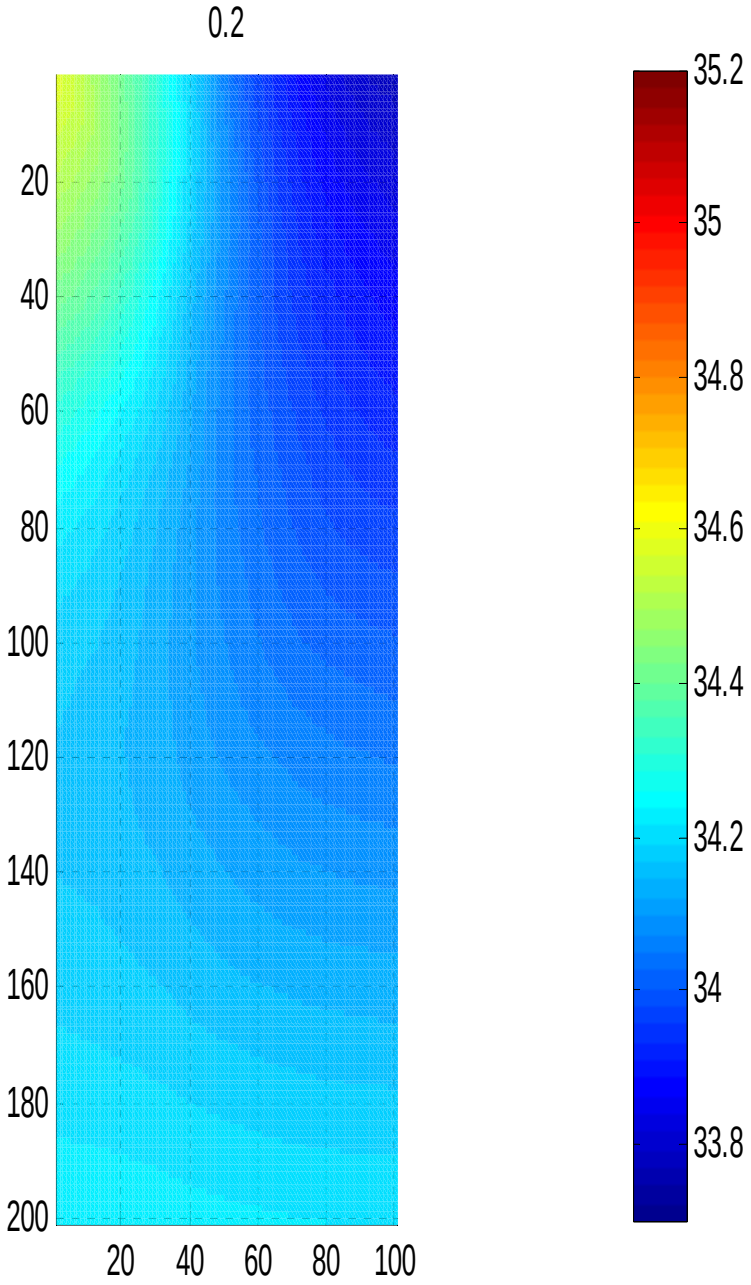

Figure 5.20 Temperature distribution at t=0.2 s

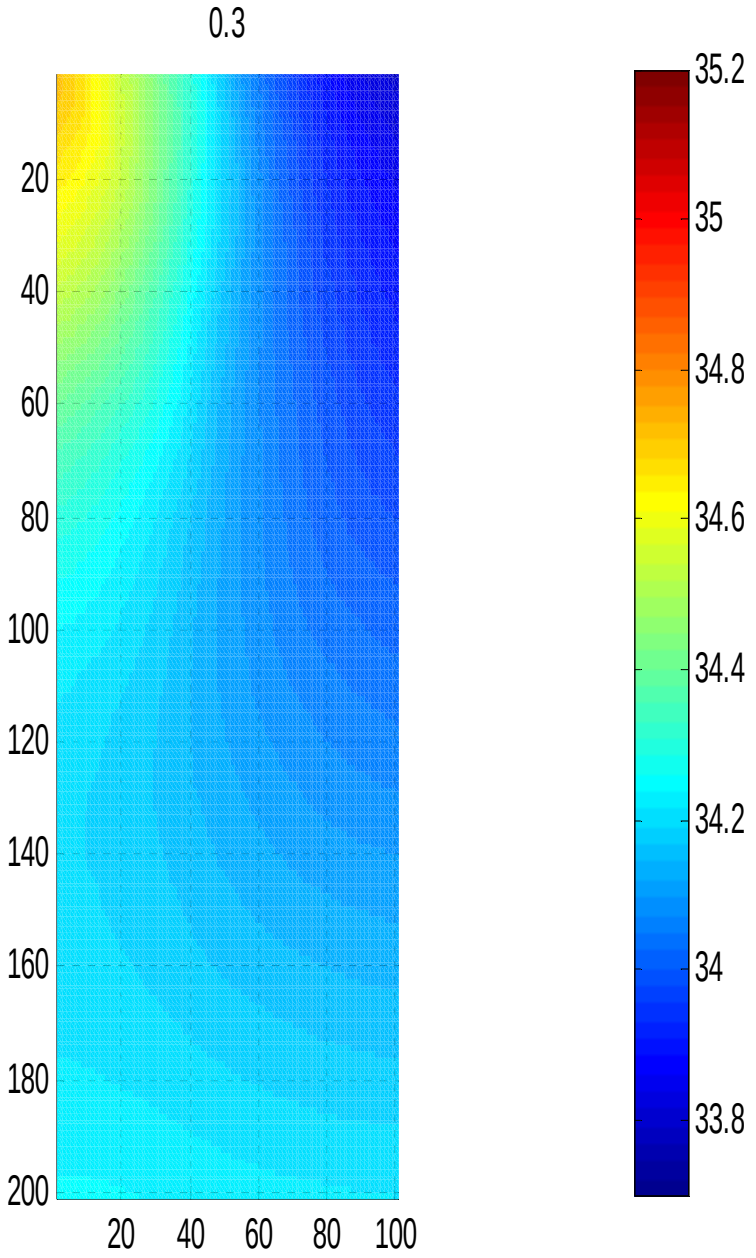

Figure 5.21 Temperature distribution at t=0.3 s

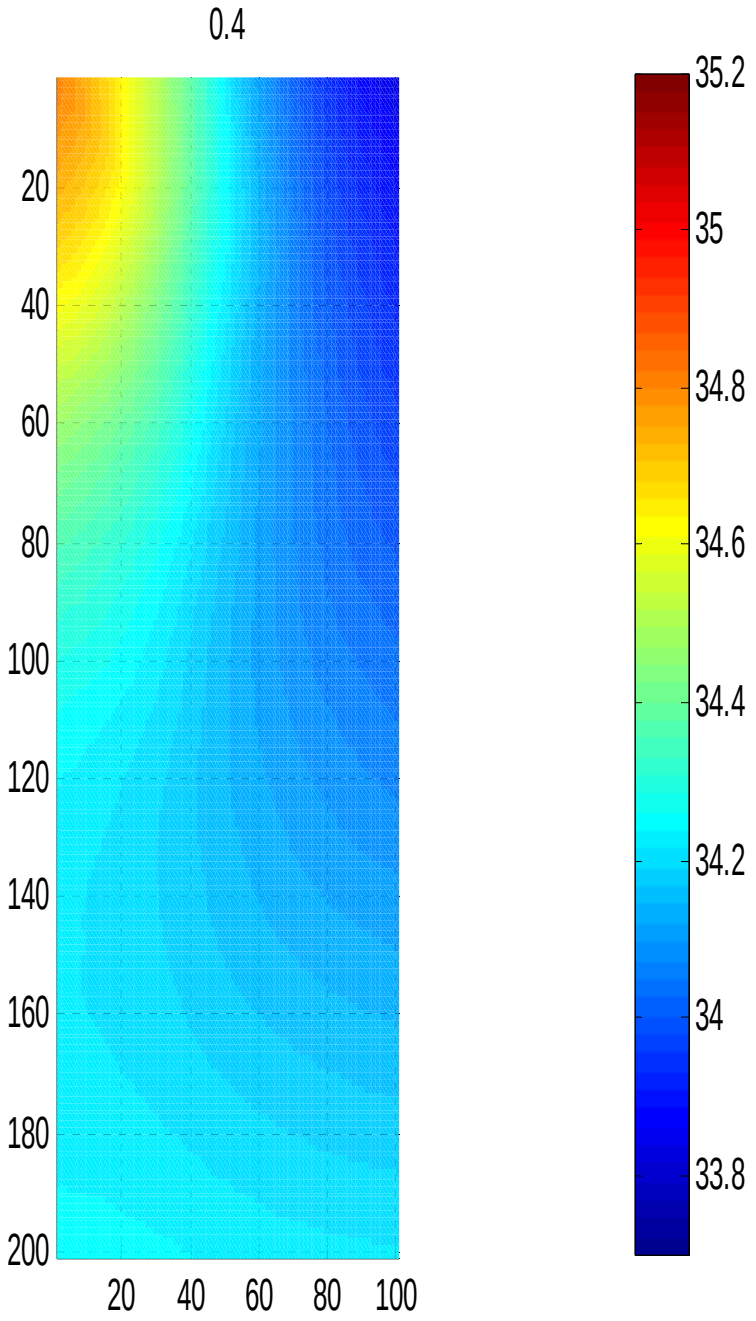

Figure 5.22 Temperature distribution at t=0.4 s

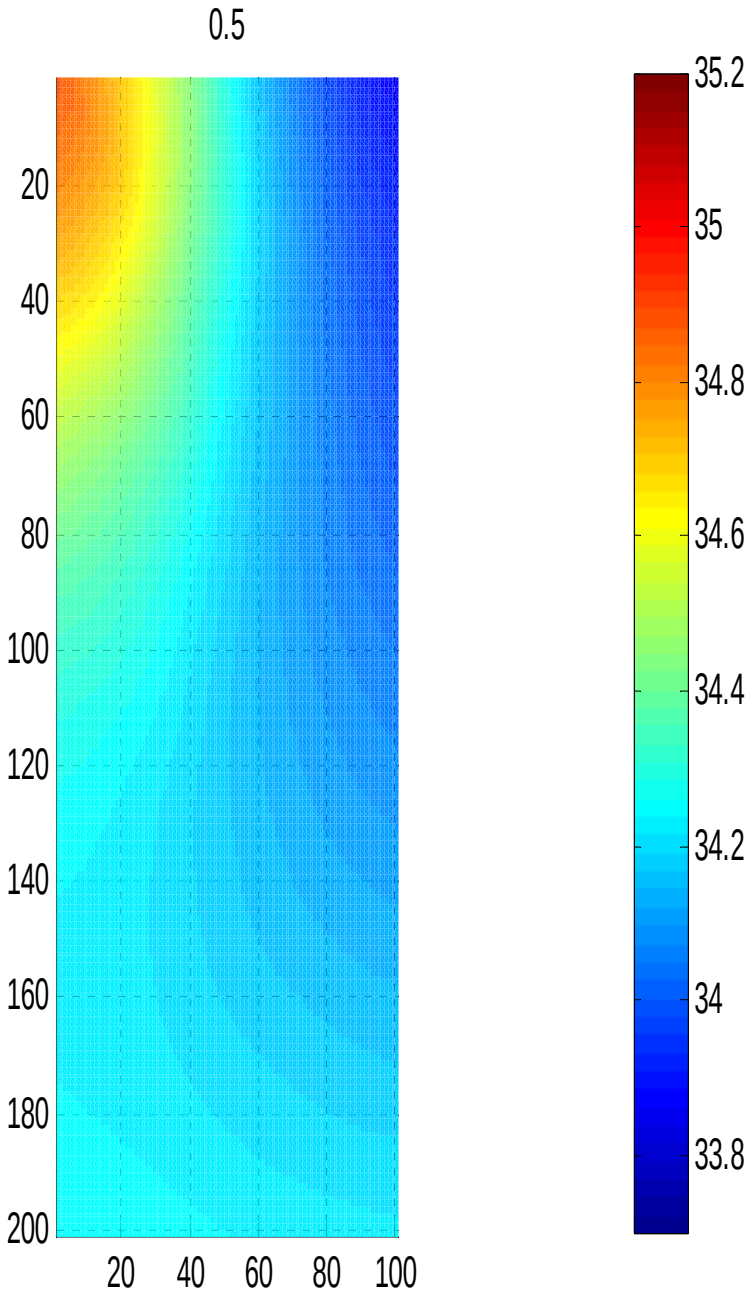

Figure 5.23 Temperature distribution at t=0.5 s

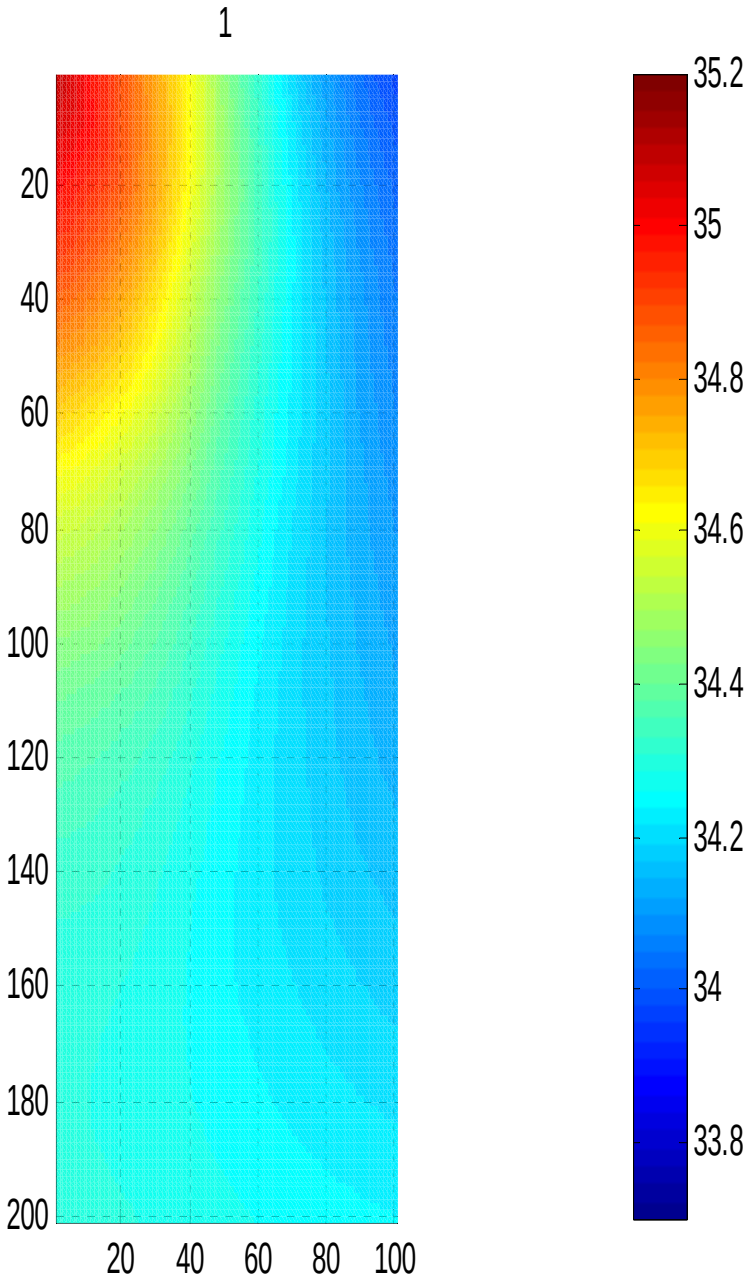

Figure 5.24 Temperature distribution at t=1 s

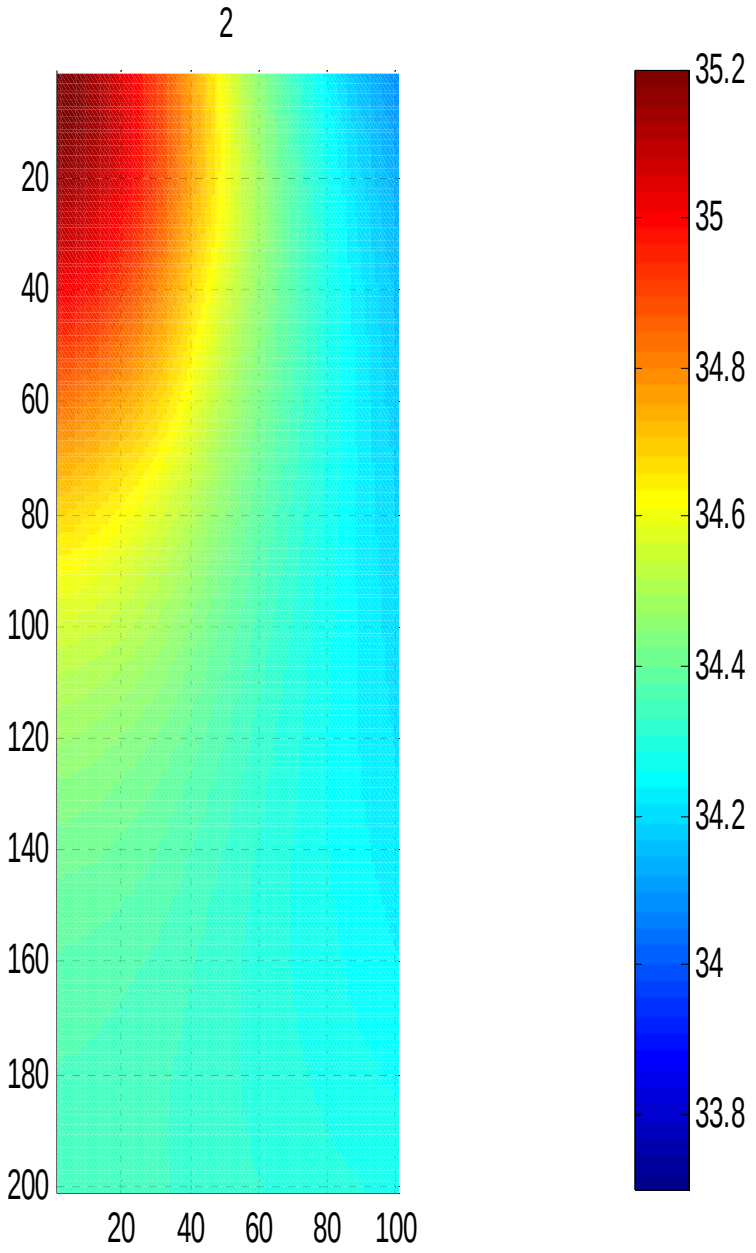

Figure 5.24 Temperature distribution at t=2 s

5.2 Single Pulse

In the next analysis, only one pulse was applied with 200 μs duration to observe the cooling curves at different points in the tissue.

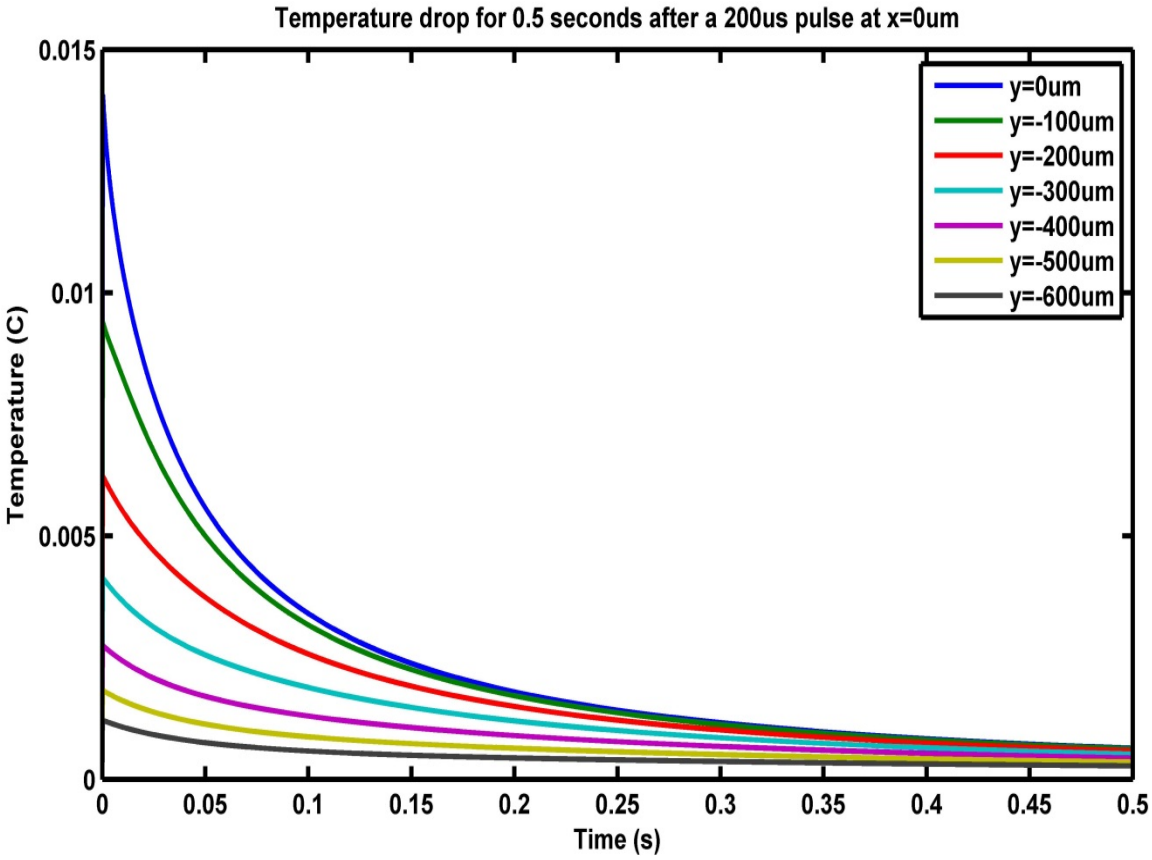

Figure 5.25 Cooling curves for 7 different points along x=0 axis after a 200 μs single pulse

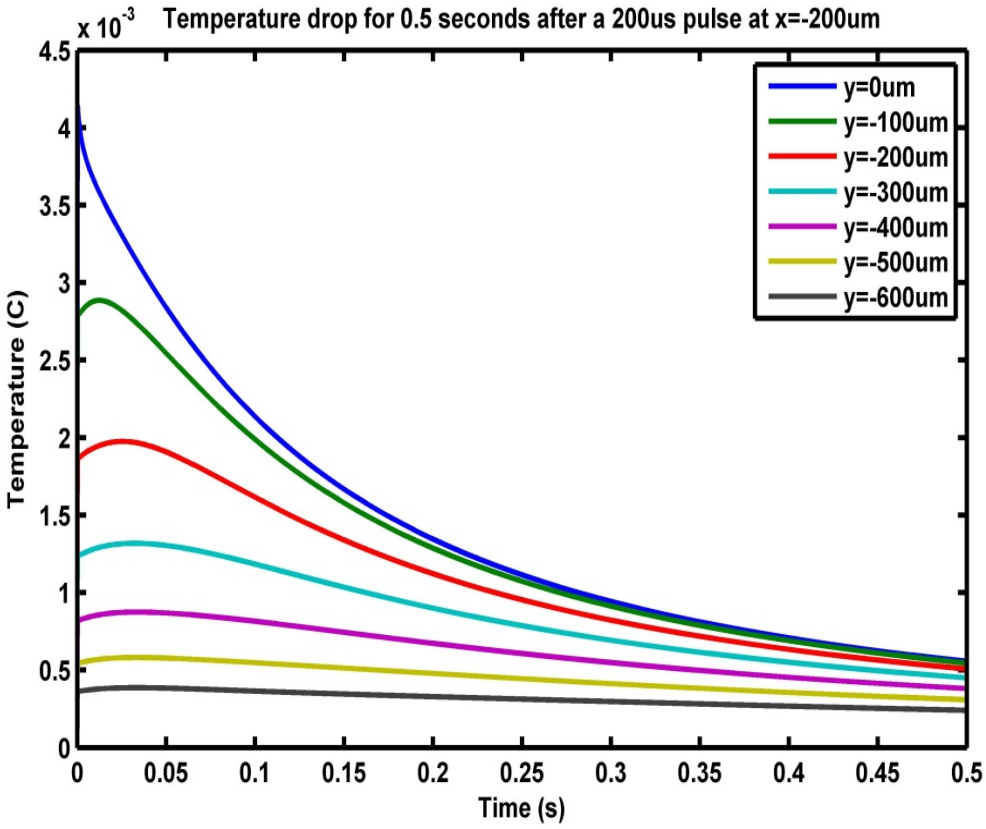

Figure 5.26 Cooling curves for 7 different points along x=200 axis after a 200 μs single pulse

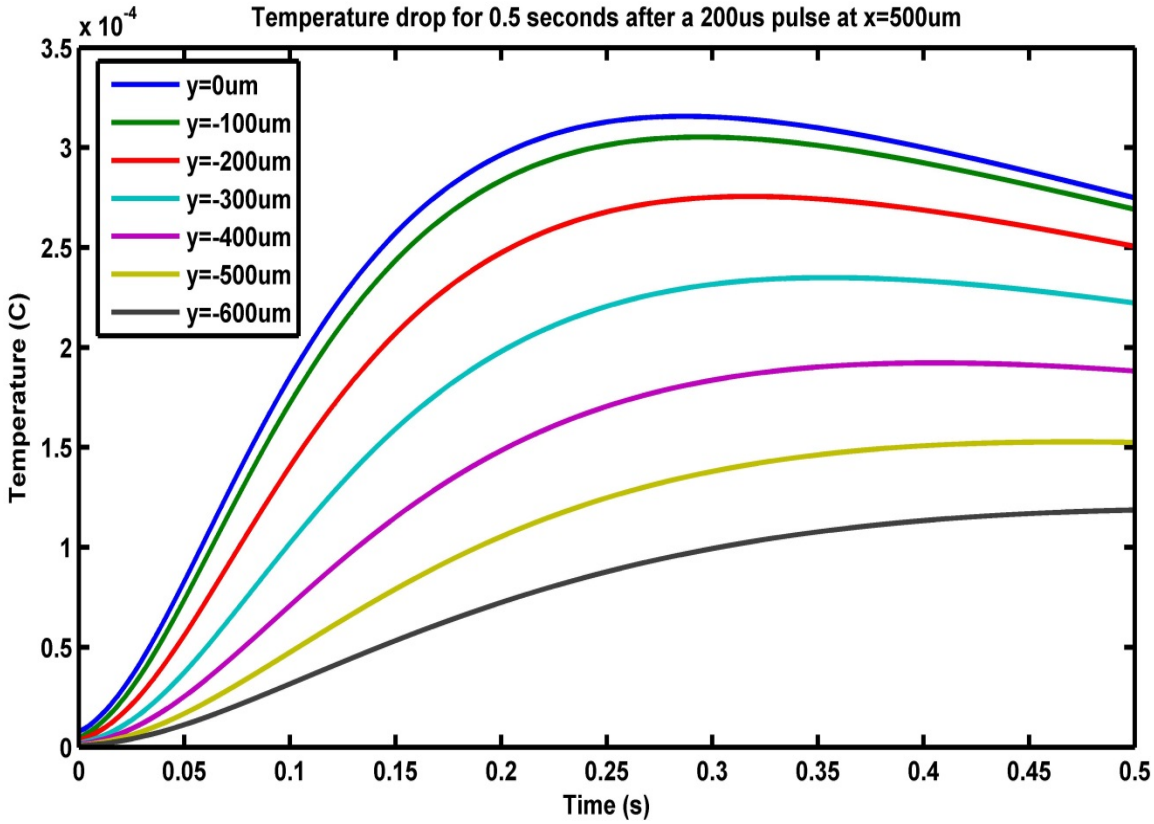

Figure 5.26 Cooling curves for 7 different points along x=500 axis after a 200 μs single pulse

CHAPTER 6

DISCUSSION, CONCLUSION AND FUTURE WORK

6.1 Results Comparison

The first sets of simulation results were compared with the experimental data (from another thesis in the laboratory) to verify the validity of our thermal model. The results were taken under the same conditions; e.g. the frequency and duty cycle. Experiments show 2.1 degree Celsius temperature increase at (0,0) and the simulation results of this study suggest a 1.9 degree at the same point. Since there are many factors that affect both experimental and simulation results, this difference is acceptable. The characteristics of the heating and cooling curves are also similar and have exponential shapes in both experimental and simulation results. The results taken so far show that the finite element model gives reliable results to continue using the model.

6.2 Temperature versus Time Plots

One of the most important results is the temperature time plots produced at different points in the tissue. These plots show the maximum and minimum temperatures of the tissue as well as the heating and cooling temporal waveforms. Figure 5.7 shows the heating characteristic of the point at (0,0) under the effect of the pulse sequence. It can be clearly seen that there is an initial rapid increase during the first 2 seconds and then the temperature increase slows down. This shows that the effect of the heat source in the tissue is higher at the initial phase of the plot then heat loss caused by blood perfusion and convection balances the temperature at after a certain point.

The data to produce the plots after Figure 5.7 were taken from deeper parts of the tissue to be able to see if the tissue characteristics differ by depth. It can be clearly seen that the initial jump of the heating curve is getting smaller with increasing depth and distance from the heat source. The heat source has the most effect on the surface and it decreases in deeper regions, so the temperature increase is smaller. After a certain point in depth the increase does not start at the same time with the laser pulse but occurs with some delay. This shows that the light source does not have a direct effect in these regions. The temperature increase is caused by the heat propagation through the tissue. The parts that are heated by the laser heat source try to cool down via thermal conduction. This heat is transferred to the neighboring tissue and the deeper parts heat up because of this thermal conduction effect. As seen on Figure 5.15, the increase starts 1.5 seconds after the pulse sequence starts and finishes 1.5 seconds later.

Another important outcome from the temperature time plots is the difference in the maximum temperatures for different pulse sequences. When the pulse sequence is changed from 20% to 50% the temperature increase becomes 2.5 times larger. Changing the duty cycle by 2.5 times causes the temperature to change by the same factor, and it can be stated that the heating effect of NIR light in the tissue is a linear function of power.

6.3 Single Pulse Plots

These plots are generated to compare the shapes of the cooling curves for different points in the tissue. The temporal characteristics of tissue heating and cooling differ by depth and distance from the center. Figure 5.25 can be used to examine the cooling characteristics at different depths within the same horizontal distance from the heat

source. The temperature values are normalized, since the starting temperatures change with depth. It can be stated that the parts that are closer to the surface reache to a higher temperature because of the increasing effect of the heat source but also cool down more quickly when the heat source is turned off due to being closer to the surface, where convectional heat loss is higher.

The points that have some horizontal distance from the laser do not show any temperature increase at the moment the laser is turned on. However, after sometime, heat conduction through the tissue causes some temperature elevation in these parts as well. This effect can clearly be seen in Figure 5.26.

6.4 Temperature Distribution Plots

These plots are generated to take the snapshot of the temperature distribution in the whole region at a specific time point in both 2D and 3D. The temperature distribution at the end of the steady state analysis is shown in Figure 5.17. Temperature difference between the surface and the deeper regions is about 1.5 degrees, and that is primarily caused by the convectional heat dissipation at the surface. After starting the pulse sequence, first the closer region heats up and the heat propagates through the tissue to the deeper parts. On Figure 5.24, the red region shows the direct effect of the laser, but because of the conductive heat transfer, the deeper parts also goes toward the blue and yellow colors, which indicate 0.5 to 1 degree temperature increase.

6.5 Conclusion

The results of this study demonstrate that it is possible to construct a thermal model of neural tissue using finite element analysis and examine the time dependent temperature distribution under the effect of an NIR laser. Contrary to the direct measurements, this procedure does not require a cumbersome experimental setup, takes less time and effort, and provides valuable insights for many potential applications. With the model, it is possible to predict the temperature values for a future experiment and calibrate the laser parameters according to these results to keep the temperature below a potentially harmful level. It is possible to change the tissue parameters for applications other than brain tissue or the light distribution function for different laser beam characteristics.

6.6 Future Work

The most influential parameters in the model are the tissue characteristics and the boundary conditions. To produce more accurate results, these parameters can be adjusted by trial and error method or by conducting some animal experiments for better determining these parameters.

Measuring the depth of the gray and white matters for the specific locations where the measurements are taken in the animals, and modeling the tissue as gray and white matters will improve accuracy as well.

REFERENCES

Abdo, A., Ersen, A., & Sahin, M. (2011). Temperature elevation inside neural tissue illuminated by NIR laser. *Conf Proc IEEE Eng Med Biol Soc*.

Bohren, C. F. a. D. R. H. (1983). *Absorption and Scattering of Light by Small Particles*: John Wiley & Sons 530 pp, Hoboken, NJ, USA.

Chylek, P. (1986). Absorption and scattering of light by small particles. *Appl Opt, 25*(18), 3166.

COMSOL Heat Transfer Module User´s Guide (2012) Comsol Inc. (pp. 296) Burlington, MA,USA.

Crochet, J. J., Gnyawali, S. C., Chen, Y., Lemley, E. C., Wang, L. V., & Chen, W. R. (2006). Temperature distribution in selective laser-tissue interaction.

Dewitt, B. L. I. (2002). *Introduction to Heat Transfer* (6 ed.): John Wiley & Sons, NJ, USA.

Gurnani, P. (2003). Near infrared spectroscopic measurement of human and animal brain structures. *Master`s thesis, University of Texas at Arlington,* Arlington, TX,USA.

Hutton, D. (2004). *Fundamentals of Finite Element Analysis* (1 ed.): Mc Graw Hill, TX, USA.

Pennes, H. H. (1948). Analysis of tissue and arterial blood temperatures in the resting human forearm. *J Appl Physiol, 1*(2), 93-122.

Pryor, R. W. (2012). *Multiphysics Modeling Using Comsol 4* (1 ed.): Mercury Learning and Information, Dulles, VA, USA.

Roylance, D. (2001). Finite Element Analysis. Master`s thesis, *Department of Materials Science and Engineering, Massachusetts Institute of Technology*.

Neuman, M. (2000). *The Biomedical Engineering Handbook*, *Physical Measurements* (2nd ed.). CRC Press LLC. Boca Raton, FL. (ch. 47).

Kreider K. (1985). *Fiber Optic Thermometry, in Applications of Radiation Thermometry, ASTM STP 895*, Philadelphia, PA. American Society of Testing Materials

Pennes, H. (1948). Analysis of tissue and arterial blood temperature in the resting human forearm, Journal of applied physiology, Vol. 1, No. 2

Eberhart R.C., (1999). *Bioheat transfer in blood-perfused tissues and clinical applications of hypothermia*, Annual review of heat transfer. Vol. 9

Gebhart, S., Lin, W., Mahadevan-Jansen A.(2006). *In vitro determination of normal and neoplastic human brain tissue optical properties using inverse adding doubling*. Phys. Med. Biol Vol. 51.

Ibrahim, T., Abraham, D, Rennaker, R. (2007). *Electromagnetic power absorption and temperature changes due to brain macine interface operation*, Ann. Biomed Vol. 35

Amin, Z., Donald, J., Masters, R., Kant, A. Steger, C., Bown, G., Lees, R. (1993). *Hepatic Metastases: Interstitial Laser Photocoagulation with Real-time US Monitoring and Dynamic CT Evaluation of Treatment*. Radiology. Vol.18

Elwassif,M., Kong, Q., Vazquez,M., Bikson, M.(2006) *Bio-heat transfer model of deep brain stimulation-induced temperature changes.* Journal of Neural Engineering.Vol. 3

Sailer, H., Shinoda,K., Blatsios, G., Kohler,K., Bondzio, L., Zrenner, E., Gekeler F. (2007). *Investigating of thermal effects of infrared lasers on the rabbit retina: a study in the course of development of an active subretinal prostheses*. Opthalmol. Vol. 245

Sharma, H., Hoopes, P. (2003). *Hyperthermia induced pathophysiology of the central nervous system*. Int. J. Hyperthermia. Vol. 19. (pp.325–354)